ARTICLE

doi:10.1038/nature19799

Frizzled proteins are colonic epithelial receptors for *C. difficile* toxin B

Liang Tao[1,2], Jie Zhang[1,2]*, Paul Meraner[3]*, Alessio Tovaglieri[4], Xiaoqian Wu[5], Ralf Gerhard[6], Xinjun Zhang[7,8], William B. Stallcup[9], Ji Miao[4,10], Xi He[7,8], Julian G. Hurdle[5], David T. Breault[4,10,11], Abraham L. Brass[3,12] & Min Dong[1,2]

***Clostridium difficile* toxin B (TcdB) is a critical virulence factor that causes diseases associated with *C. difficile* infection. Here we carried out CRISPR–Cas9–mediated genome–wide screens and identified the members of the Wnt receptor frizzled family (FZDs) as TcdB receptors. TcdB binds to the conserved Wnt–binding site known as the cysteine–rich domain (CRD), with the highest affinity towards FZD1, 2 and 7. TcdB competes with Wnt for binding to FZDs, and its binding blocks Wnt signalling. FZD1/2/7 triple–knockout cells are highly resistant to TcdB, and recombinant FZD2–CRD prevented TcdB binding to the colonic epithelium. Colonic organoids cultured from FZD7–knockout mice, combined with knockdown of FZD1 and 2, showed increased resistance to TcdB. The colonic epithelium in FZD7–knockout mice was less susceptible to TcdB–induced tissue damage *in vivo*. These findings establish FZDs as physiologically relevant receptors for TcdB in the colonic epithelium.**

Infection of the colon by the opportunistic Gram-positive bacterium *C. difficile* leads to a range of manifestations from diarrhoea to life-threatening pseudomembranous colitis and toxic megacolon[1–5]. It is the most common cause of antibiotic-associated diarrhoea and a leading cause of gastroenteritis-associated death in developed countries, accounting for nearly half a million cases and 29,000 deaths annually in the United States[6]. Two homologous exotoxins, TcdA and TcdB, are the causal agents for diseases associated with *C. difficile* infection[4,7–9]. These toxins enter cells via receptor-mediated endocytosis and inactivate small GTPases by glucosylating a key residue, resulting in cell rounding and eventual cell death[4,7,10]. Of the two toxins, TcdB alone is capable of causing the full spectrum of diseases, as $TcdA^-B^+$ strains have been clinically isolated and engineered $TcdA^-B^+$ strains induced death in animal models[11–14].

How TcdB targets the colonic epithelium remains unknown. TcdB can enter a variety of cell lines, suggesting that its receptor(s) are widely expressed in transformed cells. It has also been reported that TcdB is enriched in the heart after injection into zebrafish embryos[15]. Chondroitin sulfate proteoglycan 4 (CSPG4, also known as neuron-glial antigen 2 (NG2)) has been identified as a TcdB receptor in a short hairpin RNA (shRNA)-mediated knockdown screen[16], and was shown to be a functional receptor for TcdB in HeLa cells and in HT-29 cells, a human colorectal cell line. However, CSPG4 is not expressed in the colonic epithelium[17]. Poliovirus receptor-like 3 (PVRL3; also known as nectin-3) was recently identified from a gene-trap insertional mutagenesis screen in Caco-2 cells, a human colorectal cell line, as a factor involved in necrotic cell death (cytotoxicity) induced by TcdB[18], but whether it functions as a TcdB receptor remains to be established.

Here we carried out unbiased genome-wide screens using the CRISPR–Cas9 approach[19,20] and identified the FZDs as TcdB receptors. Using colonic organoid models and FZD7-knockout mice, we established FZDs as physiologically relevant receptors for TcdB in the colonic epithelium.

CRISPR–Cas9 screen for TcdB receptors

The C-terminal domains of TcdA and TcdB contain a region known as combined repetitive oligopeptides (CROPs) (Extended Data Fig. 1a), which can bind carbohydrates and may mediate toxin binding to cells[21]. Recent studies suggested the presence of an additional receptor-binding region beyond the CROPs[22–25]. Consistently, we found that a truncated toxin ($TcdB_{1–1830}$) lacking the CROPs induced cell rounding in various cell lines at picomolar concentrations (Extended Data Fig. 1b–d)[26]. To identify both the receptor(s) recognized by the CROPs and the receptor(s) recognized by other regions, we carried out two separate screens, with either full-length TcdB or $TcdB_{1–1830}$ (Fig. 1a).

HeLa cells that stably express RNA-guided endonuclease Cas9 were transduced with lentiviral libraries that express short guide RNAs (sgRNA) targeting 19,052 genes, with six sgRNAs per gene[19]. After four rounds of selection with increasing concentrations of toxins, the sgRNA sequences from the surviving cells were identified via next-generation sequencing (NGS). We ranked candidate genes based on the number of unique sgRNAs versus NGS reads (Fig. 1b, c, Extended Data Fig. 2 and Source Data).

UDP-glucose pyrophosphorylase (UGP2) stood out in both screens (Fig. 1b, c). UGP2 is a cytosolic enzyme producing UDP-glucose, which is used by TcdA and TcdB to glucosylate small GTPases. Mutations in UGP2 have been shown to render cells resistant to TcdA and TcdB[27,28]. Besides UGP2, the top hit from the full-length TcdB screen is CSPG4 (Fig. 1b), confirming a previous report that identified CSPG4 as a TcdB receptor[16]. The highest-ranking plasma membrane protein from the $TcdB_{1–1830}$ screen is FZD2 (Fig. 1c). FZD2 is a member of the FZD family of receptors for Wnt signalling, which is a key

[1]Department of Urology, Boston Children's Hospital, Harvard Medical School, Boston, Massachusetts 02115, USA. [2]Department of Microbiology and Immunobiology and Department of Surgery, Harvard Medical School, Boston, Massachusetts 02115, USA. [3]Department of Microbiology and Physiological Systems (MaPS), University of Massachusetts Medical School, Worcester, Massachusetts 01655, USA. [4]Division of Endocrinology, Boston Children's Hospital, Boston, Massachusetts 02115, USA. [5]Center for Infectious and Inflammatory Diseases, Texas A & M Health Science Center, Houston, Texas 77030, USA. [6]Institute of Toxicology, Hannover Medical School, 30625 Hannover, Germany. [7]The F. M. Kirby Neurobiology Center, Boston Children's Hospital, Harvard Medical School, Boston, Massachusetts 02115, USA. [8]Department of Neurology, Harvard Medical School, Boston, Massachusetts 02115, USA. [9]Tumor Microenvironment and Cancer Immunology Program, Sanford-Burnham Prebys Medical Discovery Institute, Cancer Center, La Jolla, California 92037, USA. [10]Department of Pediatrics, Harvard Medical School, Boston, Massachusetts 02115, USA. [11]Harvard Stem Cell Institute, Cambridge, Massachusetts 02138, USA. [12]Gastroenterology Division, Department of Medicine, University of Massachusetts Medical School, Worcester, Massachusetts 01655, USA.
*These authors contributed equally to this work.

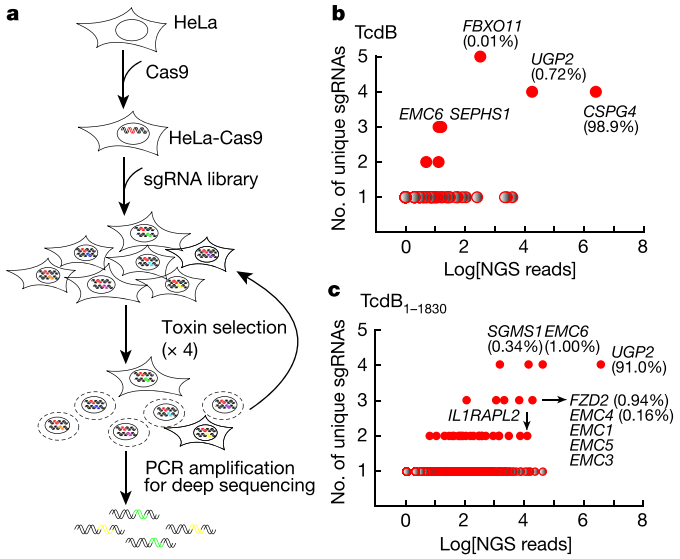

Figure 1 | Genome-wide CRISPR–Cas9-mediated screens to identify host factors for TcdB. a, Schematic drawing of the screen process. PCR, polymerase chain reaction. **b**, **c**, Genes identified in the screens with TcdB (**b**) or $TcdB_{1–1830}$ (**c**). The *y* axis is the number of unique sgRNAs for each gene. The *x* axis represents the number of sgRNA reads for each gene. The percentages of the sgRNA reads of top-ranking genes among total sgRNA reads are noted.

signalling pathway regulating proliferation and self-renewal of colonic epithelial cells[29,30]. Besides FZD2, an unusual group of high-ranking hits are subunits of the endoplasmic reticulum membrane protein complex (EMC)[31,32].

To validate the screening results, we generated *UGP2*$^{-/-}$, *CSPG4*$^{-/-}$, *FZD2*$^{-/-}$ and *EMC4*$^{-/-}$ HeLa cell lines using the CRISPR–Cas9 approach (Supplementary Table 1). Two additional knockout cells were also generated and examined: sphingomyelin synthase 1 (*SGMS1*$^{-/-}$) and interleukin-1 receptor accessory protein-like 2 (*IL1RAPL2*$^{-/-}$) (Fig. 1c). These cells were challenged with either TcdB or $TcdB_{1–1830}$ using the cytopathic cell-rounding assay[1] (Extended Data Fig. 3a, b). *UGP2*$^{-/-}$ cells were highly resistant (~3,000-fold) to both TcdB and $TcdB_{1–1830}$ compared with wild-type HeLa cells (Fig. 2a and Supplementary Table 2). *CSPG4*$^{-/-}$ cells showed increased resistance to TcdB (~240-fold), but not to $TcdB_{1–1830}$. *FZD2*$^{-/-}$ and *EMC4*$^{-/-}$ cells both showed increased resistance (~15 and ~11-fold, respectively) to $TcdB_{1–1830}$, but not to TcdB. *SGMS1*$^{-/-}$ and *IL1RAPL2*$^{-/-}$ cells did not show significant changes in sensitivity to toxins under our assay conditions. Increased resistance of *UGP2*$^{-/-}$, *CSPG4*$^{-/-}$, *FZD2*$^{-/-}$ and *EMC4*$^{-/-}$ cells was further confirmed by immunoblot analysis for glucosylation of RAC1, a small GTPase (Extended Data Fig. 3c).

CSPG4 is a CROP-dependent TcdB receptor

We next focused on CSPG4 and FZD2 as potential TcdB receptors. Binding of TcdB to *CSPG4*$^{-/-}$ cells was reduced compared with wild-type HeLa cells (Fig. 2b). Ectopic expression of rat CSPG4 restored

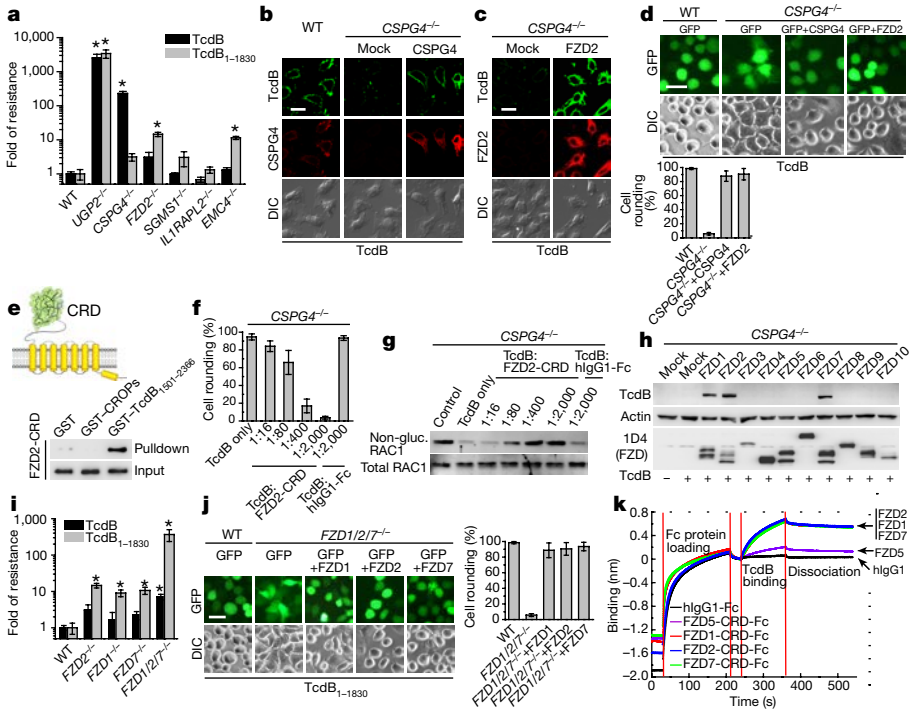

Figure 2 | FZDs are functional receptors for TcdB. a, The sensitivities of the indicated HeLa knockout cells to TcdB and $TcdB_{1–1830}$ were quantified using the cytopathic cell-rounding assay (see Extended Data Fig. 3) and normalized to wild-type (WT) HeLa cells as fold of resistance. The experiments were repeated three times. **b**, **c**, Immunostaining analysis showed that TcdB binding (10 nM, 10 min) to *CSPG4*$^{-/-}$ cells was reduced (**b**). Ectopic expression of rat CSPG4 increased binding of TcdB. Transfection of FZD2 also increased TcdB binding to *CSPG4*$^{-/-}$ cells (**c**). Scale bar, 20 μm. DIC, differential interference contrast. **d**, Ectopic expression of CSPG4 or FZD2 restored TcdB entry into *CSPG4*$^{-/-}$ cells, resulting in cell rounding (5 pM, 3 h). Green fluorescent protein (GFP)-marked transfected cells. Scale bar, 50 μm. **e**, A schematic illustration of FZD (top). Fc-tagged FZD2-CRD binds to GST-tagged $TcdB_{1501–2366}$, but not to GST-tagged CROPs. **f**, **g**, FZD2-CRD prevented TcdB (300 pM, 3 h) entry into *CSPG4*$^{-/-}$ cells, measured by the cell-rounding assay (**f**) and glucosylation (gluc.) of RAC1 (**g**). Human IgG1-Fc (hIgG1-Fc) is a control. **h**, Transfection of either FZD1, 2 or 7 increased TcdB binding (10 nM, 10 min) to *CSPG4*$^{-/-}$ cells, assayed by immunoblot analysis of cell lysates. Actin is a loading control. **i**, The sensitivities of *FZD1*$^{-/-}$, *FZD2*$^{-/-}$, *FZD7*$^{-/-}$ and *FZD1/2/7*$^{-/-}$ cells to TcdB and $TcdB_{1–1830}$ were analysed as described in **a**. **j**, Ectopic expression of FZD1, 2 or 7 restored $TcdB_{1–1830}$ entry into *FZD1/2/7*$^{-/-}$ cells (300 pM, 3 h). Scale bar, 50 μm. **k**, Characterization of TcdB binding to Fc-tagged CRDs of FZD1, 2, 5 and 7 using the BLI assay (see Supplementary Table 3 for K_d analysis). Representative images are from one of three independent experiments. Error bars indicate mean ± standard deviation (s.d.), $n = 6$, $^*P < 0.005$, *t*-test.

binding and entry of TcdB (Fig. 2b, d). TcdB binds directly to purified rat CSPG4 extracellular domain fragments (CSPG4-EC) independent of the chondroitin sulfate glycan in CSPG4 (Extended Data Fig. 4a, b). These results are consistent with a previous report[16]. However, contrary to the previous suggestion that CSPG4 does not bind to the CROPs[16], we conclude that the CROPs are essential for TcdB binding to CSPG4 because: (1) $TcdB_{1–1830}$ does not bind to either purified CSPG4-EC or CSPG4 expressed on cell surfaces (Extended Data Fig. 4b, c); (2) *CSPG4*$^{-/-}$ cells showed similar levels of sensitivity to $TcdB_{1–1830}$ as wild-type cells (Fig. 2a); and (3) the CROPs are capable of competing with TcdB for binding to CSPG4 on cell surfaces (Extended Data Fig. 4d, e). We note that the previous study used $TcdB_{1851–2366}$ as the CROPs[16]. Recent structural studies confirmed that the CROP region starts around residue 1834 instead of 1851 (ref. 33). Here we used full-length CROPs (residues 1831–2366). It is possible that the 1831–1850 region is required for TcdB binding to CSPG4.

FZDs are CROP–independent receptors

Transfecting *CSPG4*$^{-/-}$ cells with FZD2 also increased binding of TcdB (Fig. 2c) and restored entry of TcdB into *CSPG4*$^{-/-}$ cells (Fig. 2d), suggesting that FZD2 is an alternative receptor. In contrast to CSPG4, ectopically expressed FZD2 increased binding of $TcdB_{1–1830}$ and $TcdB_{1501–2366}$ on cell surfaces, but not the CROPs (Extended Data Fig. 4c, f), suggesting that it is a CROP-independent receptor. FZD2 is a seven-pass transmembrane protein and contains a sole distinct extracellular domain known as the CRD (Fig. 2e)[29]. Consistently, recombinant Fc-tagged FZD2-CRD binds directly to glutathione *S*-transferase (GST)-tagged $TcdB_{1501–2366}$, but not to the CROPs in pulldown assays (Fig. 2e).

It is possible that CSPG4 is expressed at a much higher level than FZD2 in HeLa cells, which may explain why TcdB binding to *CSPG4*$^{-/-}$ cells is barely detectable using immunostaining and immunoblot assays. Notably, TcdB can enter *CSPG4*$^{-/-}$ cells at picomolar concentrations, as detected by the sensitive cytopathic cell-rounding assay (Fig. 2f). Such entry is blocked by recombinant FZD2-CRD in a dose-dependent manner, as evidenced by a lack of cell rounding and RAC1 glucosylation (Fig. 2f, g), suggesting that endogenous FZD2 mediates TcdB binding and entry in *CSPG4*$^{-/-}$ cells.

The FZD family includes ten members (FZD1–10) in humans[29]. The ectopic expression of FZD1, 2 and 7 each increased binding of TcdB to *CSPG4*$^{-/-}$ cells (Fig. 2h and Extended Data Fig. 5a), probably because the CRDs of FZD1, 2 and 7 share ~98% sequence similarity (Extended Data Fig. 5b)[29]. Consistently, FZD7-CRD, but not FZD8-CRD, when expressed on cell surfaces via a fused glycophosphatidylinositol (GPI) anchor, mediated strong binding of TcdB to cells (Extended Data Fig. 5c).

HeLa cells express multiple FZDs[34]. We next generated FZD1 and FZD7 single-knockout HeLa cells, as well as FZD1/2/7 triple-knockout cells. *FZD1/2/7*$^{-/-}$ cells exhibited normal growth rates, probably because HeLa cells still express other FZDs. *FZD1*$^{-/-}$ and *FZD7*$^{-/-}$ cells showed reductions in sensitivity to $TcdB_{1–1830}$ similar to those of *FZD2*$^{-/-}$ cells (Fig. 2i). *FZD1/2/7*$^{-/-}$ cells were highly resistant to $TcdB_{1–1830}$ (~300-fold), confirming that FZD1, 2 and 7 all contribute to $TcdB_{1–1830}$ entry into HeLa cells. Transfection of FZD1, 2 or 7 restored $TcdB_{1–1830}$ entry into *FZD1/2/7*$^{-/-}$ cells (Fig. 2j). *FZD1/2/7*$^{-/-}$ cells also become ~10-fold more resistant to full-length TcdB than wild-type cells (Fig. 2i), indicating that endogenous FZD1, 2 and 7 are responsible for a portion of TcdB entry into wild-type HeLa cells. *FZD1/2/7*$^{-/-}$ cells showed the same level of sensitivity to TcdA as wild-type cells (Extended Data Fig. 5d), confirming that the resistance of *FZD1/2/7*$^{-/-}$ cells is specific to TcdB.

We further quantified the binding kinetics between CRDs of FZD1, 2, and 7 and TcdB using the bio-layer interferometry (BLI) assay. The results revealed a single binding site with low nanomolar affinities (dissociation constant (K_d) = 32 nM for FZD1, 19 nM for FZD2, and 21 nM for FZD7) (Fig. 2k, Extended Data Fig. 5e and Supplementary Table 3). Furthermore, FZD2-CRD showed the same binding affinity to $TcdB_{1–1830}$ (K_d = 17 nM) as to full-length TcdB (Extended Data Fig. 5f). FZD5-CRD also binds to TcdB when measured by the sensitive BLI assay, but with a much weaker affinity than FZD1, 2 and 7 (K_d = 670 nM) (Fig. 2k and Extended Data Fig. 5e). It is possible that additional FZD family members may function as low-affinity receptors for TcdB.

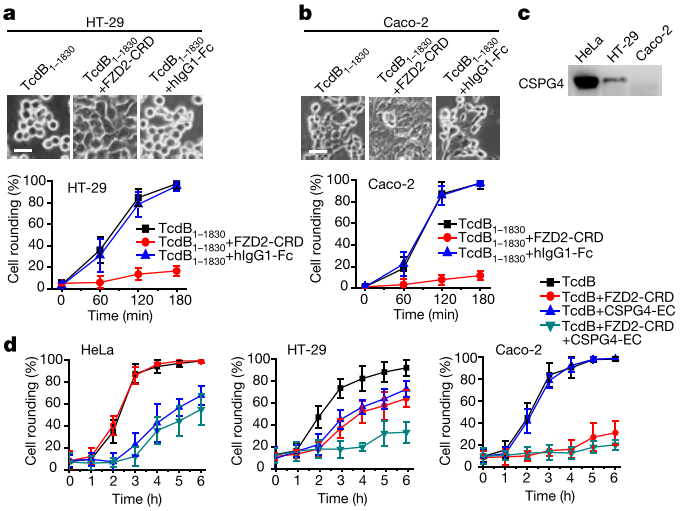

Figure 3 | FZDs versus CSPG4 in cell lines. a, **b**, FZD2-CRD protected HT-29 (**a**) and Caco-2 cells (**b**) from $TcdB_{1–1830}$ (300 pM, 3 h). Representative images are from one of three independent experiments. Scale bars: 25 μm (**a**) or 50 μm (**b**). **c**, Expression of CSPG4 in HeLa, HT-29 and Caco-2 cells was examined via immunoblot analysis of cell lysates. One experiment from four is shown. **d**, Protection from TcdB using FZD2-CRD and CSPG4-EC on HeLa (5 pM TcdB), HT-29 (50 pM TcdB) and Caco-2 (150 pM TcdB) cells was quantified by the cytopathic cell-rounding assay. Representative images are shown in Extended Data Fig. 6b. Error bars indicate mean ± s.d.

The finding that *EMC4*$^{-/-}$ cells showed a similar level of toxin resistance as *FZD2*$^{-/-}$ cells is also consistent with FZDs being TcdB receptors (Fig. 2a). Although its function remains to be established, the EMC appears to be critical for the folding/stability of multi-transmembrane proteins[35,36]. Consistently, expression of transfected FZD1, 2 or 7 was reduced in *EMC4*$^{-/-}$ cells compared with wild-type cells (Extended Data Fig. 5g, h).

CSPG4 versus FZDs in cell lines

We next addressed whether TcdB is capable of simultaneous binding to both CSPG4 and FZDs. As shown in Extended Data Fig. 6a, FZD2-CRD binds to TcdB pre-bound by immobilized CSPG4-EC on the microtitre plate, confirming that CSPG4 and FZDs do not compete with each other for binding to TcdB.

We then examined the receptors responsible for TcdB entry in HT-29 and Caco-2 cells, which are known to express multiple FZDs[37]. FZD2-CRD protected both HT-29 and Caco-2 from $TcdB_{1–1830}$ (Fig. 3a, b), suggesting that FZDs are functional receptors in these two cell lines. Interestingly, CSPG4 is expressed at high levels in HeLa, at much lower levels in HT-29, and is undetectable in Caco-2 cells (Fig. 3c). Consistently, CSPG4-EC alone was sufficient to reduce TcdB entry into HeLa cells, whereas a combination of CSPG4-EC and FZD2-CRD was required to reduce TcdB entry into HT-29 cells, and FZD2-CRD alone protected Caco-2 cells (Fig. 3d and Extended Data Fig. 6b). These data suggest that CSPG4 and FZDs represent non-competing TcdB receptors, each capable of mediating binding and entry of TcdB. Their particular contribution in a given cell type may depend on their expression levels.

We also tested the potential role of PVRL3. Ectopically expressed PVRL3 did not increase either binding or entry of TcdB into

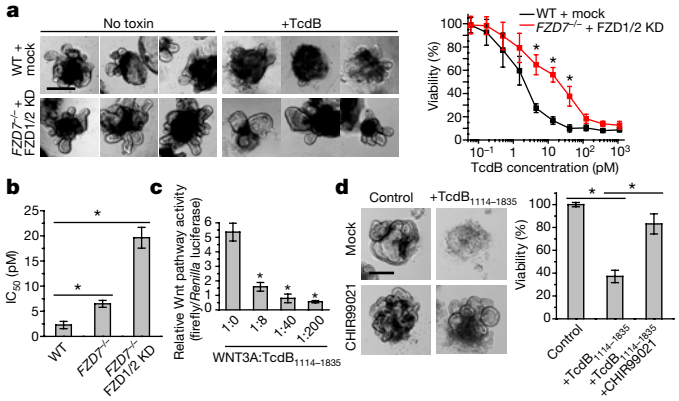

Figure 4 | FZDs are receptors for TcdB in colonic organoids. **a**, Left, three sets of representative DIC images of wild-type (WT) and *FZD7*$^{-/-}$ plus FZD1/2-knockdown (KD) organoids exposed to TcdB (0.5 pM, 3 days). Right, viability of organoids exposed to TcdB for 3 days was quantified by the MTT assay. $n = 6$, $^*P < 0.005$, *t*-test. **b**, The half-maximum inhibitory concentration (IC_{50}; the TcdB concentration that results in 50% viability after 3 days) of wild-type, *FZD7*$^{-/-}$ and *FZD7*$^{-/-}$ plus FZD1/2-knockdown organoids were quantified as described in **a**. $n = 8$, $^*P < 0.005$, one-way analysis of variance (ANOVA). **c**, $TcdB_{1114–1835}$ blocked WNT3A-mediated signalling in 293T cells. $n = 6$, $^*P < 0.005$, *t*-test. **d**, Viability of colonic organoids after exposure to $TcdB_{1114–1835}$ (25 nM), with or without CHIR99021 (5 μM), was quantified by the MTT assay. $n = 8$, $^*P < 0.005$, one-way ANOVA. Scale bars, 200 μm. Representative images are from one of three independent experiments. Error bars indicate mean ± s.d.

CSPG4$^{-/-}$ HeLa cells (Extended Data Fig. 7a, b). The recombinant ecto-domain of PVRL3 failed to protect Caco-2 cells from TcdB in the cytopathic cell-rounding assay, whereas FZD2-CRD protected cells (Extended Data Fig. 7c). Thus, PVRL3 is probably not a relevant receptor for the cytopathic effect of TcdB in HeLa and Caco-2 cells.

FZDs are TcdB receptors in colonic organoids

To determine the receptors that mediate TcdB entry into the colonic epithelium, we first used colonic organoids, an *in vitro* 'mini-gut' model that recapitulates many important features of normal colonic epithelium[38]. Exposure to TcdB caused dose-dependent atrophy and death of organoids, which was quantified using a viability assay (Fig. 4a). We found that $TcdB_{1–1830}$ and TcdB were equally potent, suggesting that CSPG4 is not a relevant receptor in colonic organoids (Extended Data Fig. 8a). It has been reported that CSPG4 is not expressed in the colonic epithelium[17], which was confirmed by immunoblot analysis of colonic organoids and isolated mouse colonic epithelium (Extended Data Fig. 8b).

We next used colonic organoids cultured from FZD7-knockout mice, combined with adenovirus-mediated knockdown of FZD1 and FZD2 (Extended Data Fig. 8c, d). FZD7 is critical for maintaining intestinal organoids, but *FZD7*$^{-/-}$ organoids can be cultured in the presence of CHIR99021, a small-molecule inhibitor of glycogen synthase kinase-3 (GSK3), which activates Wnt/β-catenin signalling downstream of FZDs[39]. *FZD7*$^{-/-}$ organoids showed threefold more resistance to TcdB than wild-type organoids (Fig. 4b). Further knockdown of FZD1/2 in *FZD7*$^{-/-}$ organoids yielded ninefold greater resistance to TcdB than wild-type organoids (Fig. 4b), demonstrating that FZDs are relevant TcdB receptors in colonic organoids.

As both TcdB and Wnt bind to the FZD-CRD, we examined whether TcdB binding competes with Wnt and inhibits Wnt signalling. We used a non-toxic TcdB fragment (residues 1114–1835), which contains the FZD-binding region but not the enzymatic domain of TcdB. This fragment blocked WNT3A-mediated signalling in 293T cells in a dose-dependent manner, demonstrated by the TOPFLASH/TK-*Renilla* dual luciferase reporter assay (Fig. 4c and Extended Data Fig. 9a), as well as by phosphorylation levels of LRP6 (a FZD co-receptor) and DVL2 (a downstream Wnt signalling component) (Extended Data Fig. 9b)[29]. $TcdB_{1114–1835}$ did not glucosylate small GTPases in colonic organoids (Extended Data Fig. 9c), yet it inhibited organoid growth and induced death (Fig. 4d and Extended Data Fig. 9d, e). The death of colonic organoids was rescued by CHIR99021, demonstrating that the effect of $TcdB_{1114–1835}$ is due to blockage of Wnt signalling. These data raised the intriguing possibility that binding of TcdB to FZDs may directly contribute to disruption of the colon epithelium by inhibiting Wnt signalling.

FZDs are TcdB receptors in colonic epithelium

Finally, we examined the colonic epithelium *in vivo*. Immunohistochemistry (IHC) analysis showed that FZD2 and FZD7 are expressed in mouse and human colonic epithelium (Fig. 5a, b and Extended Data Fig. 10a–f). In contrast, CSPG4 is predominantly expressed in the multi-nucleated intestinal sub-epithelial myofibroblasts (ISEMFs) and is not detectable in the colonic epithelium (Fig. 5c and Extended Data Fig. 10c), which is consistent with a previous report[17].

As TcdB is released into the lumen of the colon during *C. difficile* infection, we developed a model in which we injected TcdB directly into the lumen of ligated colon segments in mice (Fig. 5d), which resulted in binding and entry of TcdB into the colonic epithelium (Fig. 5e). Co-injection of FZD2-CRD largely abolished binding of TcdB (Fig. 5e), suggesting that FZDs are the dominant receptors in the colonic epithelium.

To verify further the role of FZDs *in vivo*, we turned to FZD-knockout mouse models. FZD2/7 double-knockout mice are embryonic lethal, and *FZD2*$^{-/-}$ mice also displayed developmental defects[40]. *FZD7*$^{-/-}$ mice appear to develop normally and exhibit no overt intestinal defects under basal conditions[39,40]. Thus, we chose *FZD7*$^{-/-}$ mice to assess whether a loss of a major colonic FZD member may reduce TcdB toxicity *in vivo*. To focus the analysis on the colonic epithelium and avoid the potential effects of TcdB entry into CSPG4-expressing ISEMFs, we used $TcdB_{1–1830}$ and injected the toxin into the lumen of ligated colon segments of live mice. After an 8-h incubation period, fluid accumulation was observed in wild-type mice, but was significantly reduced in *FZD7*$^{-/-}$ mice (Fig. 5f). Histological scoring revealed extensive disruption of the epithelium, inflammatory cell infiltration and oedema in wild-type mice, but much less in *FZD7*$^{-/-}$ mice (Fig. 5g and Extended Data Fig. 10g). To assess epithelial integrity further, we performed immunofluorescent analysis on colonic sections for the cell–cell junction markers claudin-3 and ZO-1. Both markers were extensively disrupted in wild-type mice after exposure to $TcdB_{1–1830}$ but remained largely intact in *FZD7*$^{-/-}$ mice (Fig. 5h and Extended Data Fig. 10h). Together, these data demonstrate that FZDs are physiologically relevant receptors for TcdB in the colonic epithelium *in vivo*.

Discussion

Our findings support a previously proposed two-receptor model for TcdB[25], but with a notable amendment: FZDs and CSPG4 may act as receptors in different cell types. CSPG4 is expressed in the ISEMFs, which are involved in diverse processes from wound healing to inflammation[41]. Although the role of ISEMFs in *C. difficile* infection remains to be established, it is conceivable that targeting these cells by TcdB could contribute to disease progression after FZD-mediated disruption of the colonic epithelium.

Our unbiased genome-wide screens revealed multiple host factors involved in all major steps of toxin actions, from receptors (FZDs and CSPG4) to acidification in endosomes (vacuolar-type H^+-ATPase)[42,43], to enzymatic activity in the cytosol (UGP2) (Extended Data Fig. 10i). Many other top-ranking hits remain to be validated, such as FBXO11 and enzymes involved in phospholipid metabolism/signalling,

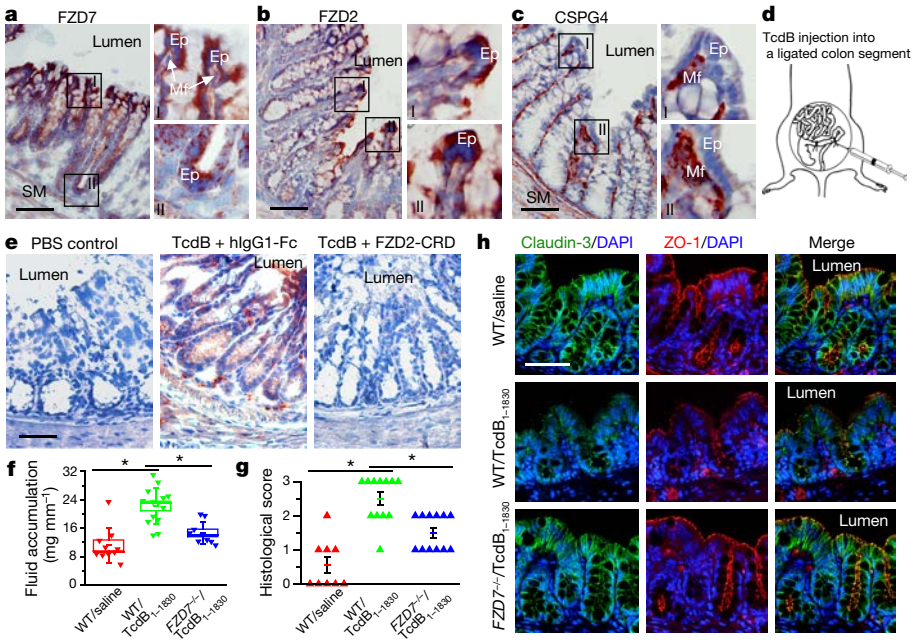

Figure 5 | FZDs are TcdB receptors in the colonic epithelium. **a**–**c**, Mouse colon cryosections were subjected to IHC analysis to detect FZD7 (**a**), FZD2 (**b**) and CSPG4 (**c**). Blue indicates cell nuclei, red indicates target proteins. Ep, epithelial cells; Mf, sub-epithelial myofibroblasts; SM, smooth muscles. **d**, A schematic illustration of the colon loop ligation assay. **e**, Co-injection of FZD2-CRD with TcdB into the ligated colonic segments prevented TcdB binding to the colonic epithelium, analysed by IHC. Red indicates TcdB and blue indicates cell nuclei. **f**–**h**, $TcdB_{1–1830}$ was injected into the ligated colonic segments and incubated for 8 h in wild-type (WT) and $FZD7^{-/-}$ mice. The colon segments were then excised and analysed for fluid accumulation (**f**), histological scoring by haematoxylin and eosin (H&E) staining (**g**; the representative images are in Extended Data Fig. 10g) and for the cell–cell junction markers claudin-3 and ZO-1 by immunofluorescent staining (**h**; blue indicates cell nuclei). DAPI, 4′,6-diamidino-2-phenylindole. Each data point represents one mouse (**f**, **g**). Boxes represent mean ± standard error of the mean (s.e.m.), and the bars represent s.d. (*$P < 0.005$, one-way ANOVA). Scale bars, 50 μm. Representative images are from one of three independent experiments.

including phosphatidylinositol 5-phosphate 4-kinase (PIP4K2B), phosphatidylinositol 4-kinase (PI4KB) and phospholipase C (PLCG1) (Extended Data Fig. 10i).

Our screen identified many key players in Wnt signalling pathways, including APC, GSK-3β, WNT5A and LRP6 (Extended Data Fig. 10i). It has been suggested that TcdA attenuates Wnt signalling in cells, although the effects appear to be indirect, largely due to deactivation of Rho GTPase by TcdA[44]. Wnt signalling is particularly important for maintaining colonic stem cells[30,45], which continuously give rise to new colonic epithelial cells. The health of these stem cells is critical for self-renewal and repair of the colonic epithelium, which has an extraordinarily fast turnover rate[45]. Our findings suggest that colonic stem cells are a major target of TcdB. The potential role of Wnt signalling inhibition in the pathogenesis of *C. difficile* infection, and the therapeutic potential of modulating Wnt signalling downstream of FZDs warrant further study. Finally, dysregulation of Wnt signalling pathways is associated with many cancers, particularly colorectal cancers[30,46]. The receptor-binding domain of TcdB, or its homologues, may serve as valuable tools and potential therapeutics for targeting Wnt signalling pathways.

Online Content Methods, along with any additional Extended Data display items and Source Data, are available in the online version of the paper; references unique to these sections appear only in the online paper.

Received 19 April; accepted 26 August 2016.
Published online 28 September 2016.

1. Lyerly, D. M., Krivan, H. C. & Wilkins, T. D. *Clostridium difficile*: its disease and toxins. *Clin. Microbiol. Rev.* **1,** 1–18 (1988).
2. Rupnik, M., Wilcox, M. H. & Gerding, D. N. *Clostridium difficile* infection: new developments in epidemiology and pathogenesis. *Nature Rev. Microbiol.* **7,** 526–536 (2009).
3. Heinlen, L. & Ballard, J. D. *Clostridium difficile* infection. *Am. J. Med. Sci.* **340,** 247–252 (2010).
4. Voth, D. E. & Ballard, J. D. *Clostridium difficile* toxins: mechanism of action and role in disease. *Clin. Microbiol. Rev.* **18,** 247–263 (2005).
5. Hunt, J. J. & Ballard, J. D. Variations in virulence and molecular biology among emerging strains of *Clostridium difficile*. *Microbiol. Mol. Biol. Rev.* **77,** 567–581 (2013).
6. Lessa, F. C. *et al.* Burden of *Clostridium difficile* infection in the United States. *N. Engl. J. Med.* **372,** 825–834 (2015).
7. Jank, T. & Aktories, K. Structure and mode of action of clostridial glucosylating toxins: the ABCD model. *Trends Microbiol.* **16,** 222–229 (2008).
8. Sun, X., Savidge, T. & Feng, H. The enterotoxicity of *Clostridium difficile* toxins. *Toxins (Basel)* **2,** 1848–1880 (2010).
9. Pruitt, R. N. & Lacy, D. B. Toward a structural understanding of *Clostridium difficile* toxins A and B. *Front. Cell. Infect. Microbiol.* **2,** 28 (2012).
10. Just, I. *et al.* Glucosylation of Rho proteins by *Clostridium difficile* toxin B. *Nature* **375,** 500–503 (1995).
11. Drudy, D., Fanning, S. & Kyne, L. Toxin A-negative, toxin B-positive *Clostridium difficile*. *Int. J. Infect. Dis.* **11,** 5–10 (2007).
12. Lyras, D. *et al.* Toxin B is essential for virulence of *Clostridium difficile*. *Nature* **458,** 1176–1179 (2009).
13. Kuehne, S. A. *et al.* The role of toxin A and toxin B in *Clostridium difficile* infection. *Nature* **467,** 711–713 (2010).
14. Carter, G. P. *et al.* Defining the roles of TcdA and TcdB in localized gastrointestinal disease, systemic organ damage, and the host response during *Clostridium difficile* infections. *MBio* **6,** e00551 (2015).
15. Hamm, E. E., Voth, D. E. & Ballard, J. D. Identification of *Clostridium difficile* toxin B cardiotoxicity using a zebrafish embryo model of intoxication. *Proc. Natl Acad. Sci. USA* **103,** 14176–14181 (2006).
16. Yuan, P. *et al.* Chondroitin sulfate proteoglycan 4 functions as the cellular receptor for *Clostridium difficile* toxin B. *Cell Res.* **25,** 157–168 (2015).
17. Terada, N. *et al.* Immunohistochemical study of NG2 chondroitin sulfate proteoglycan expression in the small and large intestines. *Histochem. Cell Biol.* **126,** 483–490 (2006).
18. LaFrance, M. E. *et al.* Identification of an epithelial cell receptor responsible for *Clostridium difficile* TcdB-induced cytotoxicity. *Proc. Natl Acad. Sci. USA* **112,** 7073–7078 (2015).
19. Shalem, O. *et al.* Genome-scale CRISPR-Cas9 knockout screening in human cells. *Science* **343,** 84–87 (2014).
20. Doudna, J. A. & Charpentier, E. The new frontier of genome engineering with CRISPR-Cas9. *Science* **346,** 1258096 (2014).
21. Greco, A. *et al.* Carbohydrate recognition by *Clostridium difficile* toxin A. *Nature Struct. Mol. Biol.* **13,** 460–461 (2006).
22. Barroso, L. A., Moncrief, J. S., Lyerly, D. M. & Wilkins, T. D. Mutagenesis of the *Clostridium difficile* toxin B gene and effect on cytotoxic activity. *Microb. Pathog.* **16,** 297–303 (1994).

23. Genisyuerek, S. *et al.* Structural determinants for membrane insertion, pore formation and translocation of *Clostridium difficile* toxin B. *Mol. Microbiol.* **79,** 1643–1654 (2011).
24. Olling, A. *et al.* The repetitive oligopeptide sequences modulate cytopathic potency but are not crucial for cellular uptake of *Clostridium difficile* toxin A. *PLoS ONE* **6,** e17623 (2011).
25. Schorch, B. *et al.* LRP1 is a receptor for *Clostridium perfringens* TpeL toxin indicating a two-receptor model of clostridial glycosylating toxins. *Proc. Natl Acad. Sci. USA* **111,** 6431–6436 (2014).
26. Ryder, A. B. *et al.* Assessment of *Clostridium difficile* infections by quantitative detection of *tcdB* toxin by use of a real-time cell analysis system. *J. Clin. Microbiol.* **48,** 4129–4134 (2010).
27. Flores-Díaz, M. *et al.* Cellular UDP-glucose deficiency caused by a single point mutation in the UDP-glucose pyrophosphorylase gene. *J. Biol. Chem.* **272,** 23784–23791 (1997).
28. Chaves-Olarte, E. *et al.* UDP-glucose deficiency in a mutant cell line protects against glucosyltransferase toxins from *Clostridium difficile* and *Clostridium sordellii*. *J. Biol. Chem.* **271,** 6925–6932 (1996).
29. MacDonald, B. T. & He, X. Frizzled and LRP5/6 receptors for Wnt/β-catenin signaling. *Cold Spring Harb. Perspect. Biol*. **4,** a007880 (2012).
30. Gregorieff, A. & Clevers, H. Wnt signaling in the intestinal epithelium: from endoderm to cancer. *Genes Dev.* **19,** 877–890 (2005).
31. Jonikas, M. C. *et al.* Comprehensive characterization of genes required for protein folding in the endoplasmic reticulum. *Science* **323,** 1693–1697 (2009).
32. Christianson, J. C. *et al.* Defining human ERAD networks through an integrative mapping strategy. *Nature Cell Biol*. **14,** 93–105 (2011).
33. Orth, P. *et al.* Mechanism of action and epitopes of *Clostridium difficile* toxin B-neutralizing antibody bezlotoxumab revealed by X-ray crystallography. *J. Biol. Chem.* **289,** 18008–18021 (2014).
34. Sagara, N., Toda, G., Hirai, M., Terada, M. & Katoh, M. Molecular cloning, differential expression, and chromosomal localization of human *Frizzled-1*, *Frizzled-2*, and *Frizzled-7*. *Biochem. Biophys. Res. Commun.* **252,** 117–122 (1998).
35. Richard, M., Boulin, T., Robert, V. J., Richmond, J. E. & Bessereau, J. L. Biosynthesis of ionotropic acetylcholine receptors requires the evolutionarily conserved ER membrane complex. *Proc. Natl Acad. Sci. USA* **110,** E1055–E1063 (2013).
36. Satoh, T., Ohba, A., Liu, Z., Inagaki, T. & Satoh, A. K. dPob/EMC is essential for biosynthesis of rhodopsin and other multi-pass membrane proteins in *Drosophila* photoreceptors. *eLife* **4,** e06306 (2015).
37. Ueno, K. *et al.* Frizzled-7 as a potential therapeutic target in colorectal cancer. *Neoplasia* **10,** 697–705 (2008).
38. Sato, T. *et al.* Single Lgr5 stem cells build crypt-villus structures *in vitro* without a mesenchymal niche. *Nature* **459,** 262–265 (2009).
39. Flanagan, D. J. *et al.* Frizzled7 functions as a Wnt receptor in intestinal epithelial Lgr5^{+} stem cells. *Stem Cell Reports* **4,** 759–767 (2015).
40. Yu, H., Ye, X., Guo, N. & Nathans, J. Frizzled 2 and Frizzled 7 function redundantly in convergent extension and closure of the ventricular septum and palate: evidence for a network of interacting genes. *Development* **139,** 4383–4394 (2012).
41. Powell, D. W. *et al.* Myofibroblasts. II. Intestinal subepithelial myofibroblasts. *Am. J. Physiol.* **277,** C183–C201 (1999).
42. Qa'Dan, M., Spyres, L. M. & Ballard, J. D. pH-induced conformational changes in *Clostridium difficile* toxin B. *Infect. Immun.* **68,** 2470–2474 (2000).
43. Pfeifer, G. *et al.* Cellular uptake of *Clostridium difficile* toxin B. Translocation of the N-terminal catalytic domain into the cytosol of eukaryotic cells. *J. Biol. Chem.* **278,** 44535–44541 (2003).
44. Bezerra Lima, B. *et al. Clostridium difficile* toxin A attenuates Wnt/β-catenin signaling in intestinal epithelial cells. *Infect. Immun.* **82,** 2680–2687 (2014).
45. Crosnier, C., Stamataki, D. & Lewis, J. Organizing cell renewal in the intestine: stem cells, signals and combinatorial control. *Nature Rev. Genet.* **7,** 349–359 (2006).
46. Gujral, T. S. *et al.* A noncanonical Frizzled2 pathway regulates epithelial-mesenchymal transition and metastasis. *Cell* **159,** 844–856 (2014).

Supplementary Information is available in the online version of the paper.

Acknowledgements We thank members of the Dong laboratory, L. Peng, X. Zhong, Q. Ma and M. Waldor for discussions; B. Ding and Y. Jing for their assistance in data analysis; N. Renzette and T. Kowalik for their advice and access to the NGS sequencer; H. Tatge for assistance on constructing toxin-expression plasmids; J. Nathans for providing FZD7 and FZD8-CRD–Myc–GPI constructs. This study was supported by National Institutes of Health (NIH) grants R01NS080833 (M.D.), R01AI091786 (A.L.B.), R01AT006732 (J.H.), R01DK084056 (D.T.B.), R01CA095287 (W.B.S.), K99DK100539 (J.M.), R01GM057603, R01GM074241 and R01AR060359 (X.H.). We also acknowledge support from the Bill and Melinda Gates Foundation (P.M. and A.L.B.), the Timothy Murphy Fund (D.T.B.), the Harvard Digestive Diseases Center (NIH P30DK034854, X.H., D.T.B. and M.D.), and the Boston Children's Hospital Intellectual and Developmental Disabilities Research Center (NIH P30HD18655, X.H., D.T.B. and M.D.). X.H. is an American Cancer Society Research Professor. M.D. and A.L.B. both hold the Investigator in the Pathogenesis of Infectious Disease Award from the Burroughs Wellcome Fund.

Author Contributions L.T., A.L.B. and M.D. conceived the project. L.T. designed and conducted the majority of the experiments. J.Z. and L.T. developed the colon loop ligation model and conducted *in vivo* experiments. P.M. and A.L.B. prepared the CRISPR library and cells for screening and contributed to the screen design and data analysis. A.T. and D.T.B. prepared colonic organoids, performed immunofluorescent experiments, and analysed data. J.M. prepared adenoviruses and assisted with knockdown experiments. X.Z. and X.H. assisted with the Wnt signalling inhibition experiments and data analysis. W.B.S. provided key reagents/advice on CSPG4. R.G., X.W. and J.G.H. provided key advice/reagents on TcdB and TcdA. L.T. and M.D. wrote the manuscript with input from all authors.

Author Information Reprints and permissions information is available at www.nature.com/reprints. The authors declare no competing financial interests. Readers are welcome to comment on the online version of the paper. Correspondence and requests for materials should be addressed to M.D. (min.dong@childrens.harvard.edu).

Reviewer Information *Nature* thanks J. Ballard, N. Fairweather and the other anonymous reviewer(s) for their contribution to the peer review of this work.

METHODS

Cell lines, antibodies and constructs. HeLa (H1, #CRL-1958), CHO (K1, #CCL-61), HT-29 (#HTB-38), Caco-2 (#HTB-37) and 293T (#CRL-3216) cells were originally obtained from ATCC. They tested negative for mycoplasma contamination, but have not been authenticated. The following mouse monoclonal antibodies were purchased from the indicated vendors: RAC1 (23A8, Abcam), non-glucosylated RAC1 (Clone 102, BD Biosciences), 1D4 tag (MA1-722, ThermoFisher Scientific), HA tag (16B12, Covance), β-actin (AC-15, Sigma), ZO-1 (339100, Life technology). Rabbit monoclonal IgG against human CSPG4 (ab139406) and rabbit polyclonal antibodies against FZD1 (ab150553), FZD2 (ab150477), FZD7 (ab51049), PVRL3 (ab63931) and claudin-3 (ab15102) were all purchased from Abcam. Rabbit monoclonal antibodies against DVL2 (30D2) and LRP6 (C5C7), and a rabbit polyclonal antibody against phosphorylated LRP6 (Ser1490) were all purchased from Cell Signaling. Chicken polyclonal IgY (#754A) against TcdB was purchased from List Biological Labs. Antibody validation is available on the manufacturers' websites. A rabbit polyclonal antibody against rodent CSPG4 and a construct expressing full-length rat CSPG4 (in pcDNA vector) were both generated in W. Stallcup's laboratory. 1D4-tagged full-length FZD1–10 constructs (in pRK5 vector) were originally generated in J. Nathans' laboratory (Baltimore, MD) and were obtained from Addgene. FZD7 and FZD8-CRD–Myc–GPI constructs were generously provided by J. Nathans and have been described previously[47]. Constructs expressing full-length human IL1RAPL2 and full-length PVRL3 were purchased from Vigene Biosciences. A construct expressing full-length mouse Syt II was described previously[48].

TcdB and other recombinant proteins. Recombinant TcdB (from *C. difficile* strain VPI 10463) and TcdA were expressed in *Bacillus megaterium* as previously described[49] and purified as His6-tagged proteins. $TcdB_{1–1830}$ was cloned into pHis1522 vector (MoBiTec) and expressed in *B. megaterium*. $TcdB_{1831–2366}$, $TcdB_{1501–2366}$ and $TcdB_{1114–1835}$ were cloned into pGEX-6P-1 or pET28a vectors and purified as GST-tagged or His6-tagged proteins in *Escherichia coli*. Rat CSPG4-EC (pool (P)1 and P2) was expressed in HEK293 cells, purified from medium with DEAE-Sepharose columns, and eluted with a gradient buffer (NaCl from 0.2 to 0.8 M, 50 mM Tris-Cl, pH 8.6) as previously described[50]. Recombinant human proteins were purchased from ACRO Biosystems (IgG1 Fc and FZD2-CRD–Fc), R&D Systems (FZD1-CRD–Fc, FZD5-CRD–Fc and FZD7-CRD–Fc), Sino Biologics (PVRL3-EC), and StemRD (WNT3A).

Generating stable HeLa-Cas9 cells and lentivirus sgRNA libraries. The human codon-optimized sequence of *S. pyogenes* Cas9 was subcloned from plasmid lenti-Cas9-Blast (Addgene #52962) into the pQCXIH retroviral vector (Clontech), which was used to generate retroviruses to transduce HeLa cells. Mixed stable cells were selected in the presence of hygromycin B (200 μg/ml, Life Technologies). Lentivirus sgRNA libraries were generated following published protocols using the human GeCKO v.2 sgRNA library (Addgene #1000000049)[19]. The GeCKO v.2 library is composed of two half-libraries (library A and library B). Each half-library contains three unique sgRNA per gene and was independently screened with toxins. Cells were transduced with lentivirus-packaged sgRNA library at a MOI of 0.2.

Screening CRISPR libraries with TcdB and $TcdB_{1–1830}$. For each CRISPR half-library of cells, 4×10^7 cells were plated onto two 15-cm culture dishes to ensure sufficient coverage of sgRNAs, with each sgRNA on average being represented about 650 times (that is, there are on average 650 cells transduced with the same sgRNA). This over-representation rate was calculated from titration plates that were set up in parallel with the library. These cells were exposed to either TcdB or $TcdB_{1–1830}$ for 48 h. Cells were then washed three times with PBS to remove loosely attached round-shaped cells. The remaining cells were re-seeded and cultured with normal medium without toxins until ~70% confluence. Cells were then subjected to the next round of screening with increased concentrations of toxins. Four rounds of screenings were carried out with TcdB (0.05, 0.1, 0.2 and 0.5 pM) and $TcdB_{1–1830}$ (5, 10, 20 and 50 pM). The remaining cells were harvested and their genomic DNA extracted using the Blood and Cell Culture DNA mini kit (Qiagen). DNA fragments containing the sgRNA sequences were amplified by PCR using primers lentiGP-1_F (AATGGACTATCATATGCTTACCGTAACTTGAAAGTATTTCG) and lentiGP-3_R (ATGAATACTGCCATTTGTCTCAAGATCTAGTTACGC). NGS (Illumina MiSeq) was performed by a commercial vendor (Genewiz).

Generating HeLa knockout cell lines. The following sgRNA sequences were cloned into LentiGuide-Puro vectors (Addgene) to target the indicated genes: CCGGAGACACGGAGCAGTGG (*CSPG4*), GCGCTGCTGGGACATCGCCT (*EMC4*), ACCTTATACCACACAACATC (*IL1RAPL2*), TGCGAGCACTTCC CGCGCCA (*FZD2*), AGCGCATGACCACTACACTG (*SGMS1*), ACAGGCA GAAAACGGCTCCT (*UGP2*), GTGTAATGACAAGTTCGCCG (*FZD1*), and GAGAACGGTAAAGAGCGTCG (*FZD7*). HeLa-Cas9 cells were transduced with lentiviruses that express these sgRNAs. Mixed populations of stable cells were selected with puromycin (2.5 μg/ml) and hygromycin B (200 μg/ml). $FZD1/2/7^{-/-}$ cells were created by sequentially transducing FZD1 and FZD7 sgRNA lentiviruses into $FZD2^{-/-}$ cells and further selected in the presence of 100 pM $TcdB_{1–1830}$. The mutagenesis rate in these mixed stable cells was determined by NGS (Supplementary Table 1).

Cytopathic assay. The cytopathic effect (cell rounding) of TcdA and TcdB was analysed using standard cell-rounding assay as previously described[1]. Briefly, cells were exposed to a gradient of TcdB and $TcdB_{1–1830}$ for 24 h. Phase-contrast images of cells were taken (Olympus IX51, ×10–20 objectives). The numbers of round-shaped and normal shaped cells were counted manually. The percentage of round-shaped cells was plotted and fitted using the Origin software.

Blocking TcdB entry into cells with CSPG4-EC and FZD2-CRD-Fc. Recombinant proteins used for cell protection assays were pre-filtered (0.22 μm, Millipore). Toxins were pre-incubated with FZD2-CRD–Fc and/or CSPG4-EC (P1) for 30 min on ice with a toxin/protein ratio of 1:400 (except when specifically noted in the figure legend). The mixtures were added into cell culture medium and cells were analysed by the cytopathic assay.

Transfection, TcdB binding to cells, and immunoblot analysis. Transient transfection of HeLa cells was carried out using PolyJet (SignaGen). Binding of TcdB to cells was analysed by exposing cells to TcdB or truncated TcdB fragments for 10 min at room temperature. Cells were washed three times with PBS and then either fixed for immunostaining analysis or harvested with RIPA buffer (50 mM Tris, 1% NP40, 150 mM NaCl, 0.5% sodium deoxycholate, 0.1% SDS, plus a protease inhibitor cocktail (Sigma-Aldrich)). Cell lysates were centrifuged and supernatants were subjected to SDS–PAGE and immunoblot analysis using the enhanced chemiluminescence method (Pierce). The full blot images are shown in Supplementary Fig. 1.

Pulldown assays. Pulldown assays were carried out using glutathione Sepharose 4B as previously described[48]. Briefly, 5 μg of GST-tagged $TcdB_{1831–2366}$ and $TcdB_{1501–2366}$ were immobilized on glutathione beads and incubated with FZD2-CRD–Fc (10 nM) for 1 h at 4 °C. Beads were then washed, pelleted, boiled in SDS sample buffer, and subjected to immunoblot analysis.

BLI assay. The binding affinities between TcdB and FZD-CRDs were measured by BLI assay using the Blitz system (ForteBio). Briefly, the CRDs-Fc of FZD1, 2, 5, 7 or human IgG1 Fc (20 μg/ml) were immobilized onto capture biosensors (Dip and Read Anti-hIgG-Fc, ForteBio) and balanced with PBS. The biosensors were then exposed to TcdB or $TcdB_{1–1830}$, followed by washing with PBS. Binding affinities (K_d) were calculated using the Blitz system software (ForteBio).

Wnt signalling assay. The TOPFLASH/TK-*Renilla* dual luciferase reporter assay was used to detect Wnt signalling activities as previously described[51]. Briefly, 293T cells in 24-well plates were co-transfected with TOPFLASH (50 ng/well), TK-*Renilla* (internal control, 10 ng/well), and pcDNA3 (200 ng/well). After 24 h, cells were exposed to WNT3A (50 ng/ml) and $TcdB_{1114–1835}$ (1:8, 1:40, and 1:200 to WNT3A) in culture medium for 6 h. Cell lysates were harvested and subjected to either firefly/*Renilla* dual luciferase assay or immunoblot analysis for detecting phosphorylated DVL2 and LRP6. Wnt signalling activates expression of TOPFLASH luciferase reporter (firefly luciferase). Co-transfected *Renilla* luciferase serves as an internal control.

Microtitre plate-based binding assay. Binding assays were performed on 96-well plates (EIA/RIA plate, Corning Costar) as described previously[50]. Briefly, microtiter plates were coated with 10 μg/ml rat CSPG4-EC proteins in coating buffer (0.1 M $NaHCO_3$, pH 8.3) at 4 °C overnight, and then blocked with 1% bovine serum albumin in PBS for 1 h. Plates were then incubated with the indicated proteins for 1 h in PBS. Wells were washed three times with PBS plus 0.05% Tween-20 at room temperature. One-step Turbo TMB (ThermoFisher Scientific) was used as the substrate, and absorbance at 450 nm was measured with a microplate reader.

Organoid culture, knockdown, and TcdB challenge assay. Crypt isolation from wild-type or $FZD7^{-/-}$ mouse colon was carried out as previously described, and organoids were expanded as spheroid cultures using conditioned medium[52]. Except for wild-type organoids used for Wnt signalling inhibition assay, CHIR99021 (3 μM) was also added to the medium[39]. Five days after passaging, organoids were re-suspended with Cell Recovery Solution (ThermoFisher Scientific) and mechanically fragmented. Fragments were transduced with adenoviruses expressing shRNA for FZD1, FZD2, or a control shRNA sequence using medium supplemented with Nicotinamide (10 mM, Sigma), Polybrene (8 μg/ml, Sigma), and Y-27632 (10 μM, Sigma), washed, and plated in growth factor-reduced Matrigel (Corning)[53]. Three days following viral transduction, organoids were challenged with TcdB by adding the toxin into the medium. Viability of organoids was quantified after 72 h.

Wnt signalling inhibition in wild-type colon organoids. $TcdB_{1114–1835}$ was added into the culture medium of wild-type colon organoids. For rescue experiments, 5 μM CHIR99021 was also added to the medium. The medium was changed every 48 h with the constant presence of $TcdB_{1114–1835}$ and/or CHIR99021. Viability of cells was analysed after 6 days.

Generating FZD1 and FZD2-knockdown adenovirus. All shRNAs were purchased from Sigma (MISSION shRNA library). The knockdown efficiency was validated as described in Extended Data Fig. 8c, d. shRNA sequences showing the highest efficiency were selected to generate adenoviruses. Adenoviruses expressing a control shRNA (5′-CTGGACTTCCAGAAGAACA-3′), shRNAs against mouse FZD1 (shRNA#2: 5′-TGGTGTGCAACGACAAGTTTG-3′), or FZD2 (shRNA#5: 5′-CGCTTCTCAGAGGACGGTTAT-3′) were constructed using the Block-it U6 adenoviral RNAi system (Life Technologies), followed by viral packaging and multiple rounds of amplification in 293A cells (Life Technologies).

Viability assay for colonic organoids. The viability of colonic organoids was assessed using the MTT assay as previously described[54]. Briefly, the MTT solution was added to the organoid culture (500 μg/ml). After incubation at 37 °C for 2 h, the medium was discarded. For each well (containing 20 μl of Matrigel, in a 48-well plate), 60 μl of 2% SDS solution was added to solubilize the Matrigel (1 h, 37 °C), followed by the addition of 300 μl of dimethylsulfoxide (DMSO) to solubilize reduced MTT (2 h, 37 °C). The absorbance at 562 nm was measured on a microplate reader. Twenty microlitres of Matrigel without organoids was used as blank control. Normal organoids without exposure to toxins were considered as 100% viable.

IHC, immunofluorescence and histology analysis. Colons from adult mice (C57BL/6 strain (purchased from The Jackson Laboratory, #000664), 10–12 weeks old, both male and female mice were used and randomly distributed into experimental groups) were dissected out and subjected to cryosectioning into sections 8–10 μm thick. Colonic sections were fixed in cold acetone for 5 min and then washed three times with PBS. The colonic sections were then blocked with 5% goat serum in PBS for 30 min at room temperature and incubated with primary antibodies overnight (anti-TcdB: 1:600; anti-FZDs: 1:250; rabbit anti-CSPG4: 1:250), followed with biotinylated goat anti-chicken or rabbit IgG secondary antibodies (1:200, Vector Laboratory) for 1 h at room temperature. The sections were then incubated with horseradish peroxidase (HRP)-conjugated streptavidin (1:500, DAKO) for 30 min. Immunoreactivity was visualized as red colour with 3-amino-9-thyl carbazole (DAKO). Cell nuclei were labelled blue with Gill's haematoxylin (1:3.5, Sigma). Frozen human colon tissue slides were purchased from BioChain Institute and subjected to IHC analysis. Immunofluorescence analysis of claudin-3 and ZO-1 was carried out using mouse colon tissues fixed in 10% formalin and embedded in paraffin (anti-claudin-3: 1:100; anti-ZO-1: 1:100). Confocal images were captured with the Ultraview Vox Spinning Disk Confocal System. Histology analysis was carried out with H&E staining of paraffin-embedded sections. Stained sections were coded and scored by observers blinded to experimental groups, based on disruption of the colonic epithelium, inflammatory cell infiltration and oedema, on a scale of 0 to 3 (mild to severe). No statistical methods were used to predetermine sample size.

Competition assays in colonic tissues with recombinant proteins. All procedures were conducted in accordance with the guidelines approved by the Boston Children's Hospital Institutional Animal Care and Use Committee (IACUC) (#3028). TcdB (40 nM) was pre-incubated with either human IgG1-Fc or FZD2-Fc (2.4 μM) for 30 min on ice. To generate the *ex vivo* colon segments, mice (C57BL/6, 6–8 weeks, both male and female mice were used, repeated three times, each time four mice per group, the experiments were not randomized or blinded) were euthanized and the colon exposed via laparotomy. A segment in the ascending colon (~2 cm long) was sealed by tying both ends with silk ligatures. The toxin samples (40 μl) were injected through an intravenous catheter into the sealed colon segment. The injection site was then sealed with a haemostat. The colon was covered with PBS-soaked gauze for 2 h, then excised and its lumen flushed with PBS three times, and subjected to IHC analysis.

Colon loop ligation assay. All procedures were conducted in accordance with the guidelines approved by the Boston Children's Hospital IACUC (#3028). Wild-type or *FZD7*$^{-/-}$ mice (The Jackson Laboratory, #012825, strain B6;129-*Fzd7*$^{tm1.1Nat}$/J, 6–8 weeks old, sample size indicated in Fig. 5f, g, both male and female mice were used, the experiments were not randomized or blinded) were anaesthetized following overnight fasting. A midline laparotomy was performed to locate the ascending colon and seal a ~2 cm loop with silk ligatures. Two micrograms of $TcdB_{1-1830}$ in 80 μl of normal saline or 80 μl of normal saline were injected through an intravenous catheter into the sealed colon segment, followed by closing the wounds with stitches. Mice were allowed to recover. After 8 h, mice were euthanized and the ligated colon segments were excised, weighed, and measured. The colon segments were fixed, paraffin-embedded, sectioned, and subjected to either H&E staining for histological score analysis or immunofluorescent staining for claudin-3 and ZO-1.

47. Hsieh, J. C., Rattner, A., Smallwood, P. M. & Nathans, J. Biochemical characterization of Wnt-Frizzled interactions using a soluble, biologically active vertebrate Wnt protein. *Proc. Natl Acad. Sci. USA* **96,** 3546–3551 (1999).
48. Dong, M. *et al.* Synaptotagmins I and II mediate entry of botulinum neurotoxin B into cells. *J. Cell Biol.* **162,** 1293–1303 (2003).
49. Yang, G. *et al.* Expression of recombinant *Clostridium difficile* toxin A and B in *Bacillus megaterium*. *BMC Microbiol.* **8,** 192 (2008).
50. Tillet, E., Ruggiero, F., Nishiyama, A. & Stallcup, W. B. The membrane-spanning proteoglycan NG2 binds to collagens V and VI through the central nonglobular domain of its core protein. *J. Biol. Chem.* **272,** 10769–10776 (1997).
51. MacDonald, B. T., Yokota, C., Tamai, K., Zeng, X. & He, X. Wnt signal amplification via activity, cooperativity, and regulation of multiple intracellular PPPSP motifs in the Wnt co-receptor LRP6. *J. Biol. Chem.* **283,** 16115–16123 (2008).
52. Miyoshi, H. & Stappenbeck, T. S. *In vitro* expansion and genetic modification of gastrointestinal stem cells in spheroid culture. *Nature Protocols* **8,** 2471–2482 (2013).
53. Wang, N. *et al.* Adenovirus-mediated efficient gene transfer into cultured three-dimensional organoids. *PLoS ONE* **9,** e93608 (2014).
54. Grabinger, T. *et al.* Ex vivo culture of intestinal crypt organoids as a model system for assessing cell death induction in intestinal epithelial cells and enteropathy. *Cell Death Dis.* **5,** e1228 (2014).

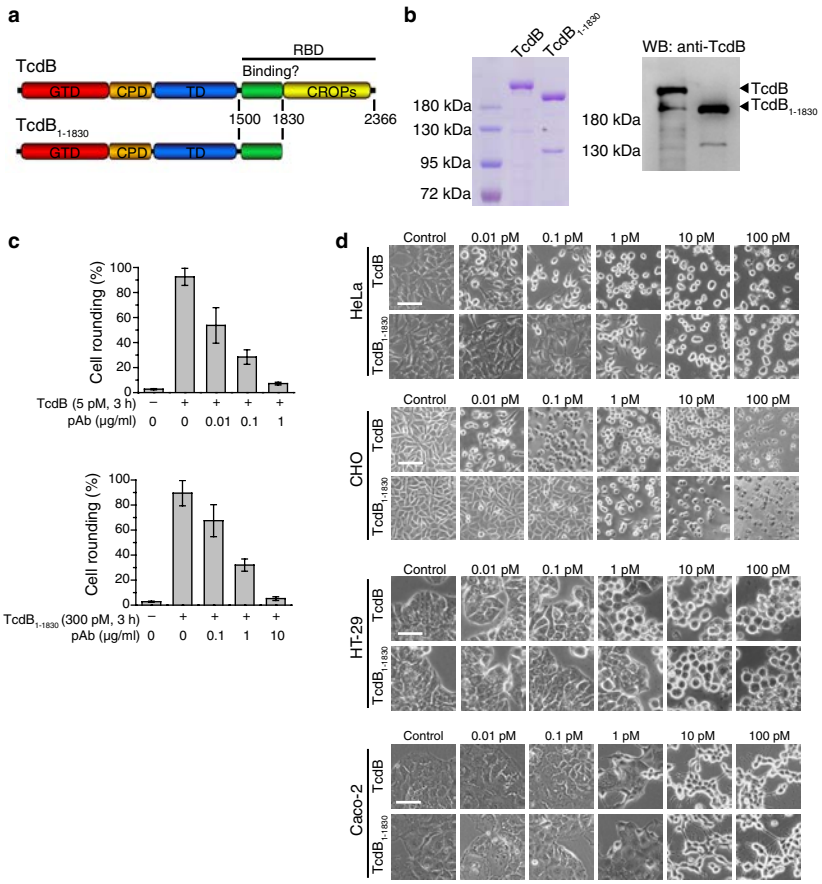

Extended Data Figure 1 | Recombinant TcdB and $TcdB_{1–1830}$. **a**, Schematic drawings of TcdB and a truncated TcdB lacking the CROP region ($TcdB_{1–1830}$). CPD, cysteine protease domain; GTD, glucosyltransferase domain; RBD, receptor-binding domain, including a putative receptor-binding region and the CROPs region; TD, translocation domain. **b**, Coomassie blue staining (left) and immunoblot (right; chicken polyclonal TcdB antibody) showing TcdB and $TcdB_{1–1830}$ recombinantly expressed in *Bacillus megaterium*. We note that $TcdB_{1–1830}$ contains a contaminating protein visible on Coomassie blue-stained gel. Mass spectrometry analysis confirmed that this band is not a fragment of TcdB. The top matching protein is the bacterial chaperone protein ClpB. **c**, Cytopathic toxicity of recombinant TcdB and $TcdB_{1–1830}$ on HeLa cells was neutralized by anti-TcdB polyclonal antibody (pAb), confirming that the toxicity is from TcdB and $TcdB_{1–1830}$ (error bars indicate mean ± s.d., two independent experiments). **d**, HeLa, CHO, HT-29, and Caco-2 cells were exposed to TcdB or $TcdB_{1–1830}$ as indicated for 24 h. $TcdB_{1–1830}$ induced cell rounding at picomolar concentrations. Scale bars: 25 µm (HT-29) or 50 µm (HeLa, CHO and Caco-2). Representative images are from one of three independent experiments.

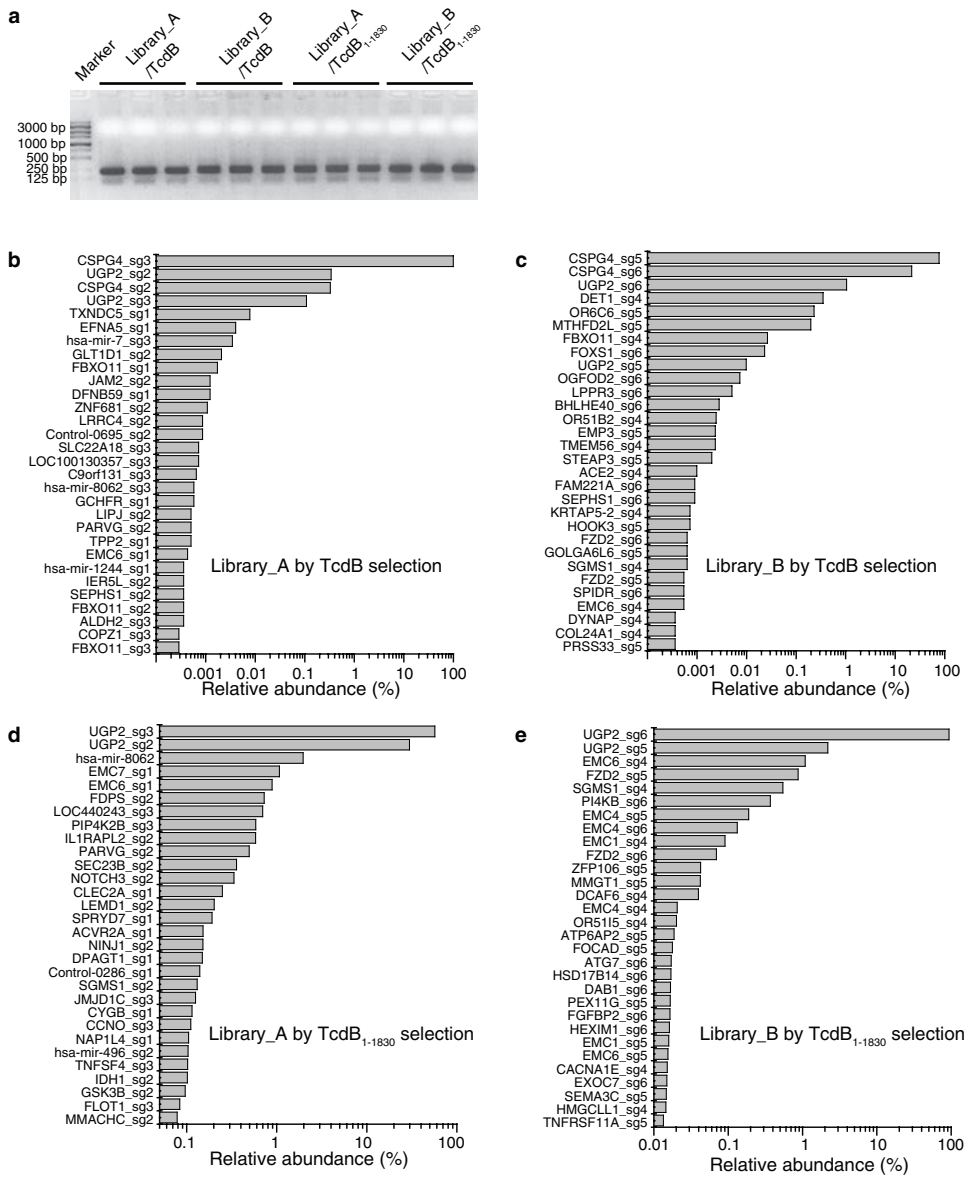

Extended Data Figure 2 | Top-ranking sgRNAs. a, Sequences of sgRNA were amplified by PCR after screening and subjected to NGS. The GeCKO v.2 sgRNA library is composed of two half libraries (library A and library B). Each half library contains three unique sgRNA per gene. These two half libraries were prepared and subjected to screens independently. **b**–**e**, Lists of top-ranking sgRNAs. See Source Data for lists of all identified sgRNAs.

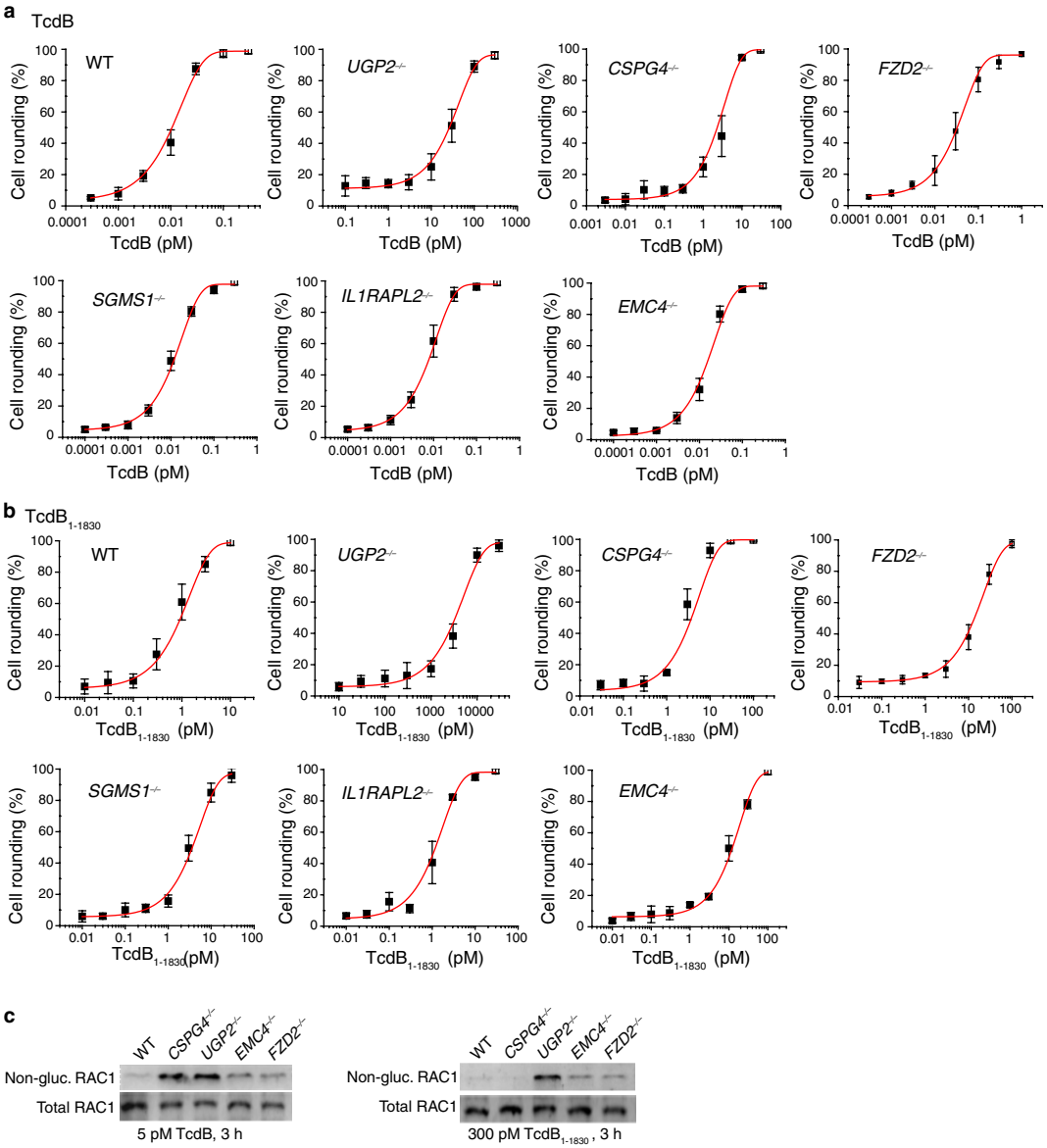

Extended Data Figure 3 | Assessing the sensitivity of HeLa knockout cells to TcdB and $TcdB_{1–1830}$. **a**, **b**, HeLa-Cas9 cells with the indicated genes mutated via CRISPR–Cas9, as well as wild-type (WT) Hela-Cas9 cells, were exposed to TcdB (**a**) or $TcdB_{1–1830}$ (**b**) for 24 h. The percentages of rounded cells were quantified and plotted (error bars indicate mean ± s.d., three independent experiments). **c**, HeLa knockout cells were exposed to TcdB or $TcdB_{1–1830}$ for 3 h. Cell lysates were subjected to immunoblot analysis for RAC1 and non-glucosylated (gluc.) RAC1. *UGP2*$^{-/-}$ cells retained high levels of non-glucosylated RAC1 after exposure to TcdB or $TcdB_{1–1830}$. *CSPG4*$^{-/-}$ cells retained high levels of non-glucosylated RAC1 after exposure to TcdB. *FZD2*$^{-/-}$ and *EMC4*$^{-/-}$ cells showed slightly higher levels of non-glucosylated RAC1 compared to wild-type cells after exposure to $TcdB_{1–1830}$. Representative blots are one from two independent experiments.

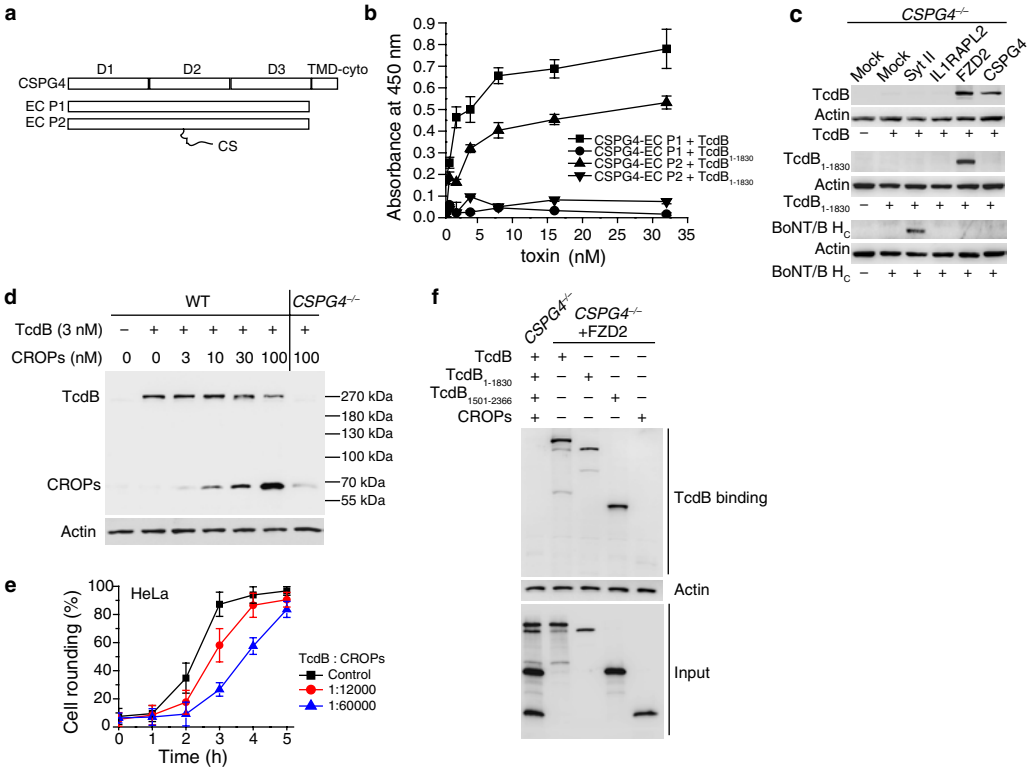

Extended Data Figure 4 | CROPs are essential for TcdB binding to CSPG4, but not required for TcdB binding to FZDs. a, Schematic drawings of rat CSPG4. Two pools of recombinant extracellular domain (EC) fragments were used: one that does not contain chondroitin sulfate (CS) chains (EC P1), and the other that contains CS (EC P2). TMD-cyto, transmembrane and cytoplasmic domain. **b**, TcdB, but not $TcdB_{1–1830}$, binds directly to both EC P1 and EC P2 of CSPG4 in a microtitre plate-based binding assay (error bars indicate mean ± s.d., two independent experiments). **c**, *CSPG4*$^{-/-}$ cells transfected with the indicated constructs were exposed to TcdB (10 nM), $TcdB_{1–1830}$ (10 nM), or the receptor-binding domain of botulinum neurotoxin B (BoNT/BH_C; 100 nM) for 10 min. Cell lysates were collected and subjected to immunoblot analysis. IL1RAPL2 and synaptotagmin II (Syt II, a receptor for BoNT/B) served as controls. Transfection of CSPG4 increased binding of TcdB, but not $TcdB_{1–1830}$, whereas transfection of FZD2 increased binding of both TcdB and $TcdB_{1–1830}$. One of three independent experiments is shown. **d**, The CROP domain binds to CSPG4 on cell surfaces in a dose-dependent manner. High concentrations of recombinant CROPs reduced CSPG4-dependent binding of TcdB to cell surfaces, indicating that the CROPs can compete with TcdB for binding to CSPG4 on cell surfaces. One of three independent experiments is shown. **e**, The CROP domain reduced cytopathic toxicity of TcdB (5 pM) on wild-type (WT) HeLa cells (error bars indicate mean ± s.d., two independent experiments). **f**, *CSPG4*$^{-/-}$ cells were transfected with FZD2 and then exposed to TcdB or indicated TcdB fragments. FZD2-mediated binding of TcdB, $TcdB_{1–1830}$ and $TcdB_{1501–2366}$, but not the CROPs ($TcdB_{1831–2366}$). One of three independent experiments is shown.

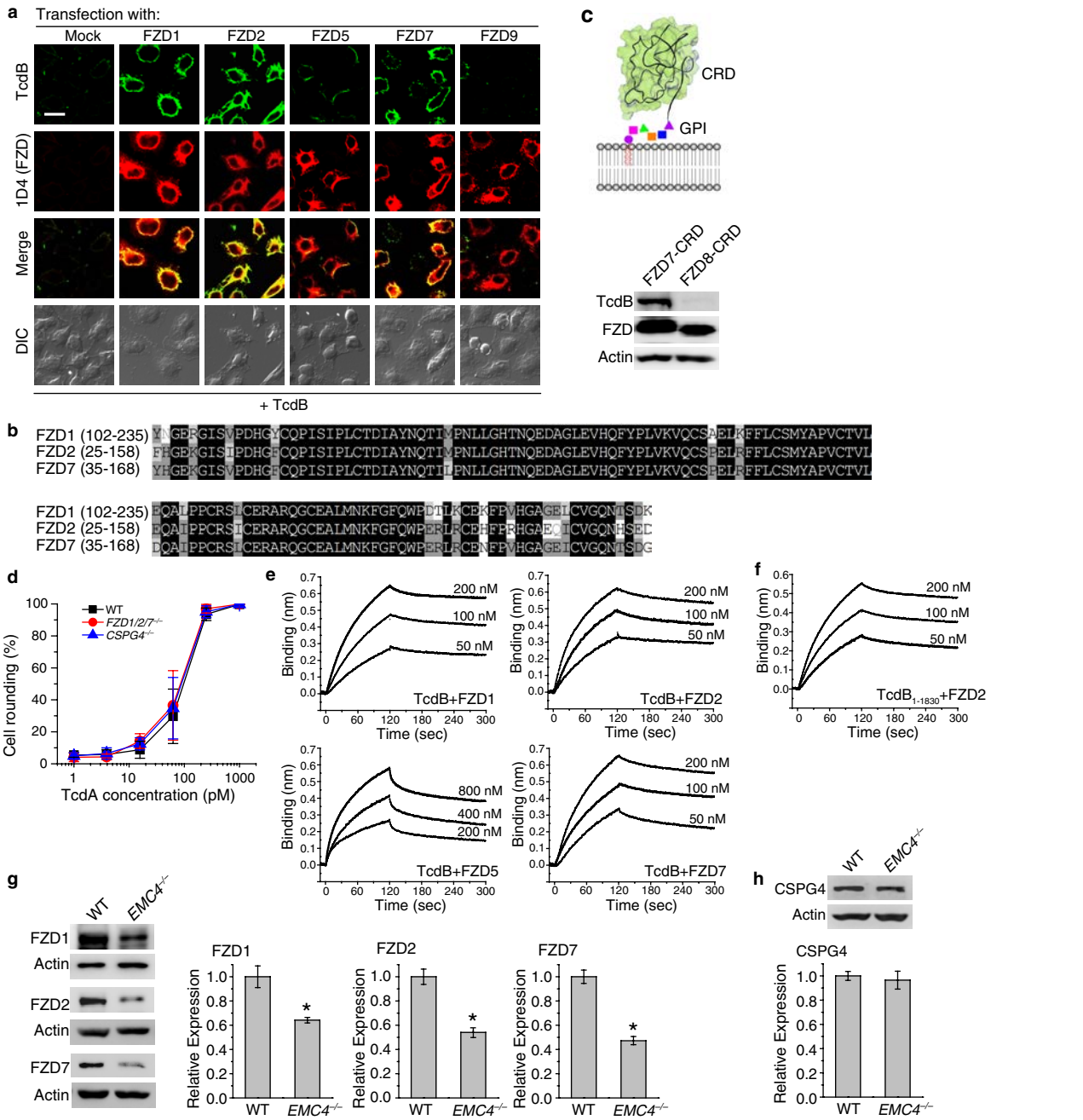

Extended Data Figure 5 | Characterizing TcdB binding to FZDs. a, *CSPG4*$^{-/-}$ cells were transfected with 1D4-tagged FZD1, 2, 5, 7 and 9. Cells were exposed to TcdB (10 nM, 10 min), washed, fixed, permeabilized and subjected to immunostaining analysis. Scale bar, 20 μm. One of three independent experiments is shown. **b**, The CRD domains of human FZD1 (residues 102–235), FZD2 (residues 25–158) and FZD7 (residues 35–168) were aligned using the Vector NTI software. **c**, FZD7-CRD, but not FZD8-CRD, when expressed on the surface of *CSPG4*$^{-/-}$ cells via a GPI anchor, mediated binding of TcdB (10 nM, 10 min) to cells. One of three independent experiments is shown. **d**, Wild-type (WT) HeLa cells, *FZD1/2/7*$^{-/-}$ cells, and *CSPG4*$^{-/-}$ cells were exposed to TcdA and subjected to cytopathic cell-rounding assay. No reduction in sensitivity to TcdA was observed for *FZD1/2/7*$^{-/-}$ cells or *CSPG4*$^{-/-}$ cells, suggesting that TcdA does not use FZD1/2/7 or CSPG4 as its receptors (error bars indicate mean ± s.d., two independent experiments). **e**, **f**, Representative binding/dissociation curves for TcdB binding to Fc-tagged CRDs of FZD1, 2, 5 and 7 (**e**), and for $TcdB_{1-1830}$ binding to FZD2-CRD-Fc (**f**). Binding parameters are listed in Supplementary Table 3. Representative curves are from one of three independent experiments. **g**, Wild-type and *EMC4*$^{-/-}$ cells were transfected with 1D4-tagged FZD1, 2 or 7. Cell lysates were subjected to immunoblot analysis. Expression of FZD1, 2 and 7 are reduced in *EMC4*$^{-/-}$ cells compared to wild-type cells ($n = 6$, $^*P < 0.005$, one-way ANOVA). Representative blots are from one of three independent experiments. **h**, Expression levels of CSPG4 in *EMC4*$^{-/-}$ cells is similar to those in wild-type cells, suggesting that EMC is not required for single-pass transmembrane proteins. One of three independent experiments is shown.

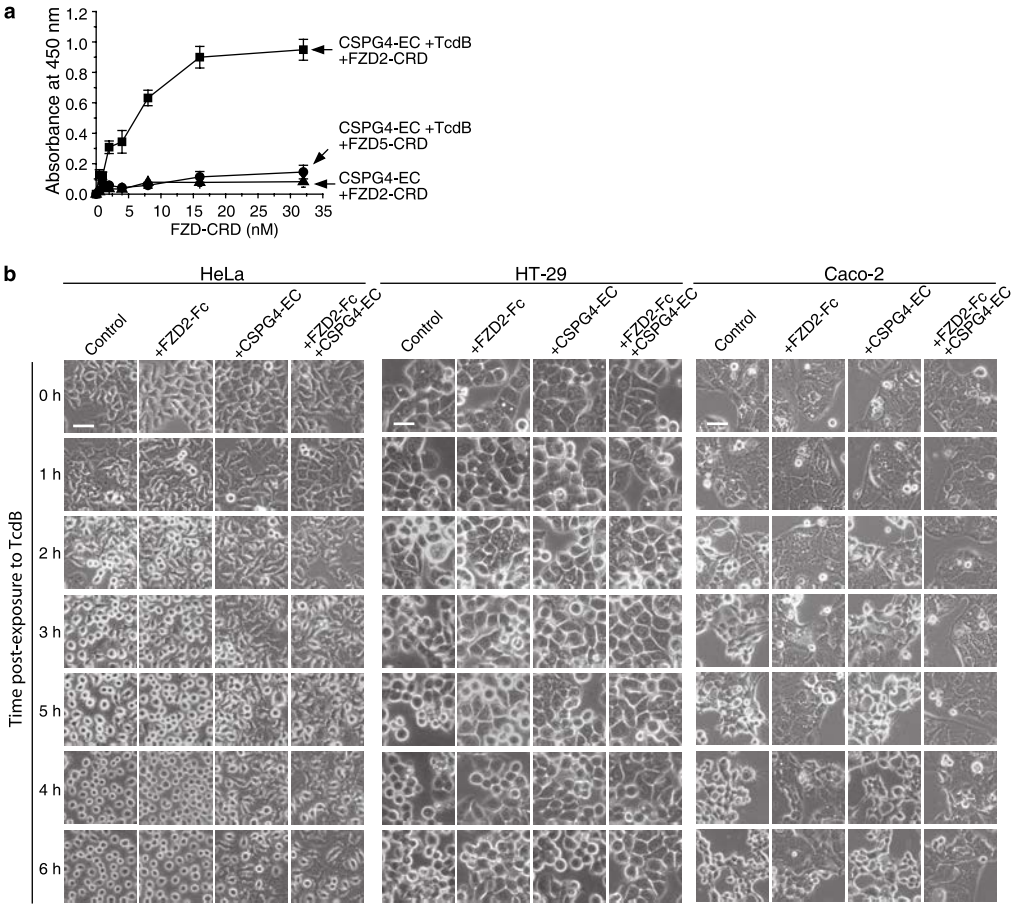

Extended Data Figure 6 | TcdB can bind to both FZD and CSPG4 simultaneously. a, Rat CSPG4-EC was immobilized on microtitre plates, followed by binding of TcdB, washing away unbound TcdB, and addition of FZD-CRD. FZD2-CRD binds robustly to TcdB that is pre-bound by CSPG4-EC on the microtitre plate. FZD2-CRD did not bind to CSPG4-EC without TcdB, and FZD5-CRD showed no detectable binding to CSPG4–TcdB in this assay (error bars indicate mean ± s.d., two independent experiments). **b**, Experiments are described in Fig. 3d on HeLa (5 pM TcdB), HT-29 (50 pM TcdB) and Caco-2 cells (150 pM TcdB). Scale bars: 50 μm (HeLa and Caco-2) or 25 μm (HT-29). Representative images are from one of four independent experiments.

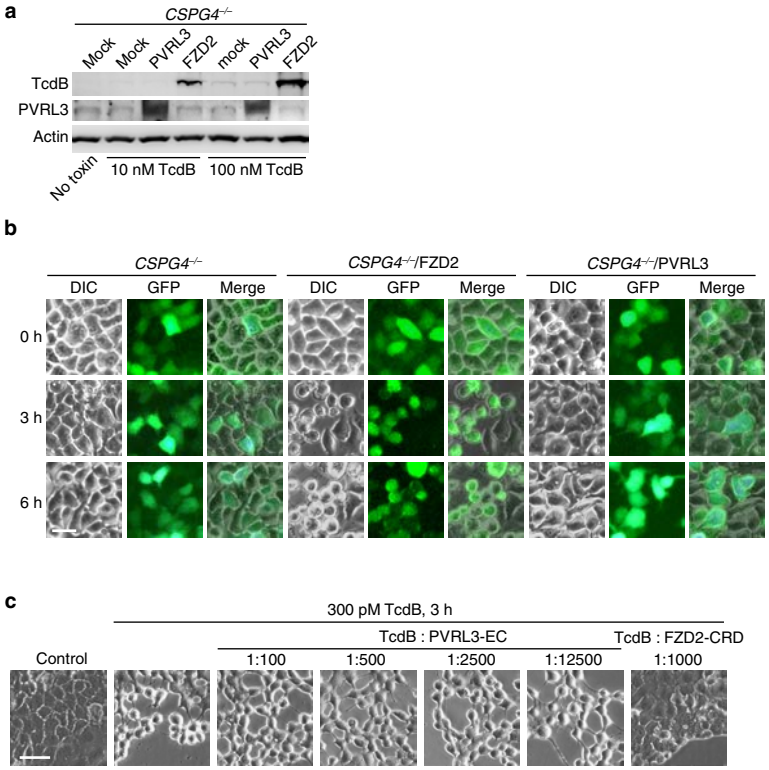

Extended Data Figure 7 | PVRL3 failed to mediate binding and entry of TcdB in HeLa and Caco-2 cells. a, *CSPG4*$^{-/-}$ HeLa cells transfected with the indicated constructs were exposed to TcdB in medium for 10 min. Cell lysates were collected and subjected to immunoblot analysis. Expression of PVRL3 was confirmed using an anti-PVRL3 antibody. Transfection of FZD2, but not PVRL-3, increased binding of TcdB to *CSPG4*$^{-/-}$ cells. One of three independent experiments is shown. **b**, Cells were challenged with TcdB (300 pM). Ectopic expression of PVRL3 failed to restore the sensitivity of *CSPG4*$^{-/-}$ HeLa cells towards TcdB, while expression of FZD2 restored entry of TcdB and resulted in rounding of transfected cells. Co-transfected GFP marked transfected cells. Scale bar, 50 μm. One of three independent experiments is shown. **c**, Recombinant extracellular domain of PVRL3 (PVRL3-EC) did not reduce TcdB entry into Caco-2 cells, analysed by the cytopathic cell-rounding assay. In contrast, FZD2-CRD prevented entry of TcdB into Caco-2 cells. Scale bar, 50 μm. One of three independent experiments is shown.

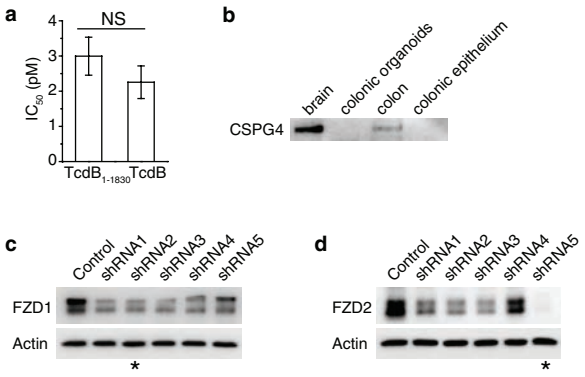

Extended Data Figure 8 | Colonic organoids showed similar levels of sensitivity to TcdB and $TcdB_{1–1830}$, and validation of FZD1 and FZD2 knockdown efficiency. a, Colonic organoids were cultured from wild-type mice. They were exposed to a gradient of TcdB or $TcdB_{1–1830}$. Viability of organoids was quantified using the MTT assay. TcdB and $TcdB_{1–1830}$ showed similar IC_{50} values, suggesting that wild-type organoids are equally susceptible to TcdB and $TcdB_{1–1830}$ ($n = 8$, error bars indicate mean ± s.d., two independent experiments). NS, not significant. **b**, Immunoblot analysis of CSPG4 expression in mouse brain, colonic organoids, mouse whole colon tissue, and isolated mouse colonic epithelium (200 μg cell/tissue lysates). The colonic epithelium was isolated from colon tissues by EDTA treatment (10 mM, 2 h at 4 °C). One of three independent experiments is shown. **c**, **d**, shRNA sequences targeting FZD1 and FZD2 were validated by measuring knockdown efficiency of transfected 1D4-tagged FZD1 and FZD2 in 293T cells. shRNAs marked with asterisks (shRNA2 for FZD1 and shRNA5 for FZD2) were used to generate adenoviruses. Actin served as the loading control. One of two independent experiments is shown.

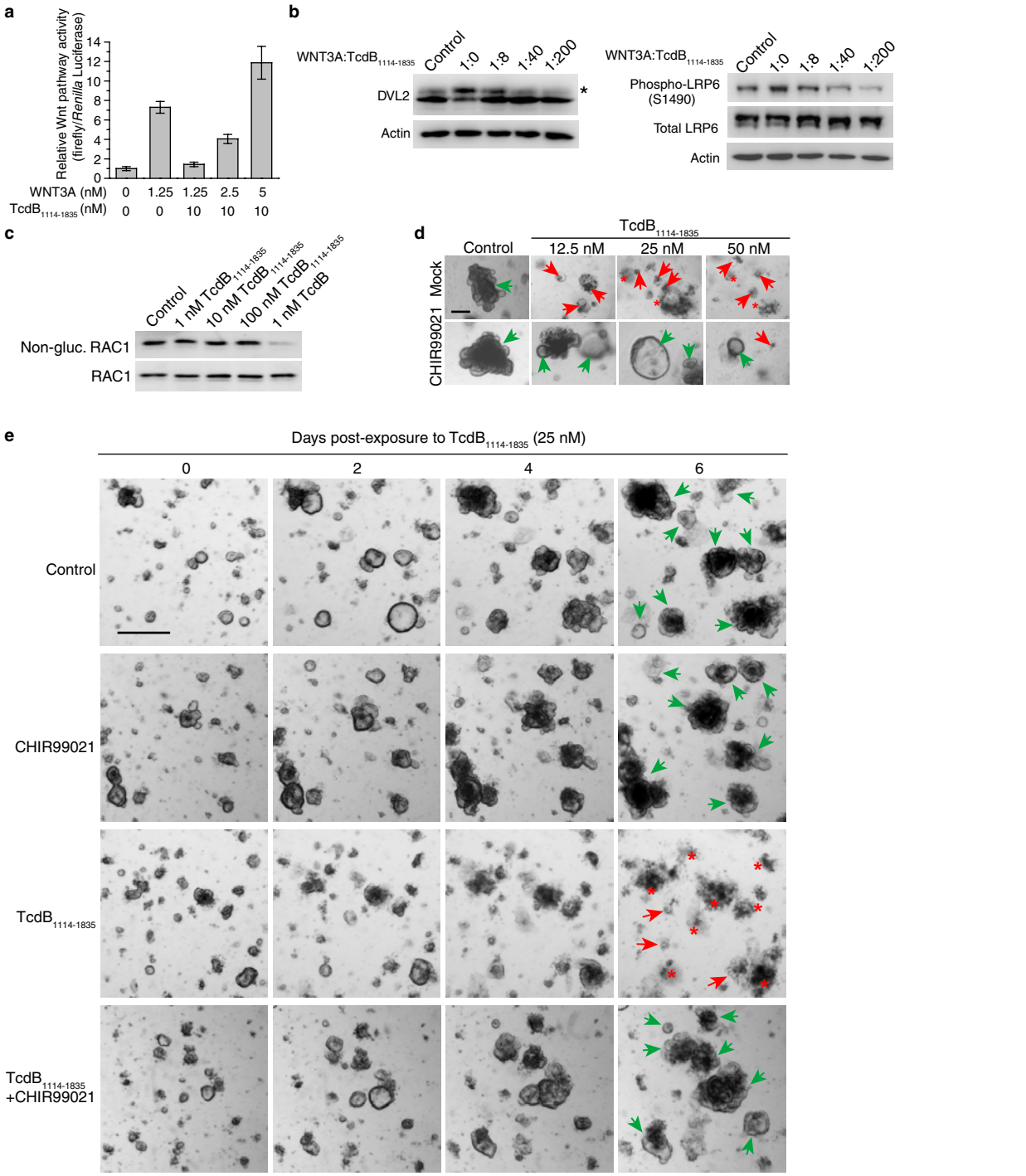

Extended Data Figure 9 | $TcdB_{1114–1835}$ inhibits Wnt signalling and induces death of colonic organoids. a, $TcdB_{1114–1835}$ blocked WNT3A-mediated signalling in 293T cells in a dose-dependent manner. Increasing concentrations of WNT3A restored Wnt reporter activity blocked by $TcdB_{1114–1835}$. Wnt signalling activity was analysed using the TOPFLASH/TK-*Renilla* dual luciferase reporter assay (error bars indicate mean ± s.d., two independent experiments). We note that 1.25 nM WNT3A equals 50 ng ml^{-1} concentration used in Fig. 4c. **b**, 293T cells in 24-well plates were exposed to WNT3A (50 ng ml^{-1}) and $TcdB_{1114-1835}$ in culture medium for 6 h. Cell lysates were harvested and subjected to immunoblot analysis for detecting phosphorylated DVL2 and LRP6. Wnt signalling activation results in phosphorylation of DVL2 and LRP6. Phosphorylated DVL2 is marked with an asterisk. One of three independent experiments is shown. **c**, Mouse colonic organoids were exposed to TcdB or $TcdB_{1114–1835}$ for 12 h. Cell lysates were subjected to immunoblot analysis. No glucosylation (gluc.) of RAC1 was observed in organoids treated with $TcdB_{1114–1835}$. One of two independent experiments is shown. **d**, Colonic organoids were exposed to $TcdB_{1114–1835}$ for 72 h, with or without CHIR99021 (5 μM). Normal organoids (green arrow), growth inhibited organoids (red arrow), and disrupted/dead organoids (asterisk) are indicated. Scale bar, 200 μm. One of three independent experiments is shown. **e**, Time-course images of colonic organoids exposed to CHIR99021 (5 μM), $TcdB_{1114–1835}$ (25 nM) or a combination of $TcdB_{1114–1835}$ plus CHIR99021, at 0, 2, 4 and 6 days. Normal organoids (green arrow), growth inhibited organoids (red arrow), and disrupted/dead organoids (asterisk) are indicated. Scale bar, 500 μm. One of four independent experiments is shown.

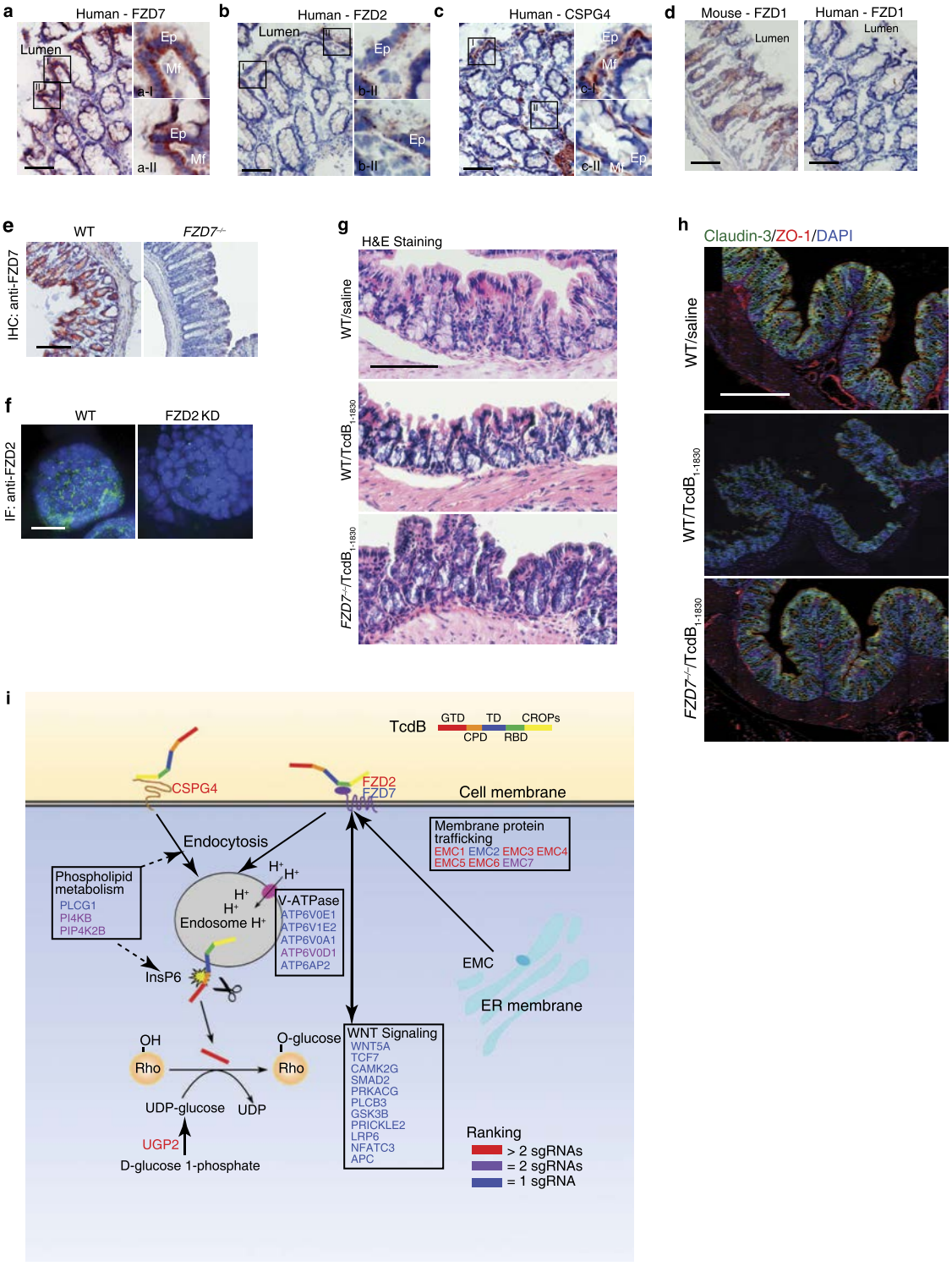

Extended Data Figure 10 | See next page for caption.

Extended Data Figure 10 | FZDs are receptors for TcdB in the colonic epithelium. a–c, Human colon cryosections were obtained from a commercial vendor and subjected to IHC analysis for detecting FZD7 (**a**), FZD2 (**b**) and CSPG4 (**c**). Ep, epithelial cells; Mf, sub-epithelial myofibroblasts. Scale bar, 50 μm. Representative images are from one of three independent experiments. **d**, Expression of FZD1 is not detectable in mouse or human colonic tissues. One of three independent experiments is shown. **e**, FZD7 antibody labelled wild-type colonic sections, but showed no signals on colonic tissues from *FZD7*$^{-/-}$ mice in IHC analysis, confirming the specificity of this antibody. One of three independent experiments is shown. **f**, Immunostaining of FZD2 (green) is reduced in FZD2-knockdown colonic organoids compared to control organoids, confirming the specificity of FZD2 antibody. Cell nuclei were labelled by DAPI (blue). Scale bar, 30 μm. One of three independent experiments is shown. **g**, Experiments are described in Fig. 5g. Representative images from one of three independent experiments are shown. Scale bar, 100 μm. **h**, Experiments were carried out as described in Fig. 5h. Low-magnification images of immunofluorescent staining of the cell–cell junction markers claudin-3 (green) and ZO-1 (red) were stitched together to show an overview of the colon tissue. The middle panel (WT/TcdB$_{1–1830}$) showed disruption of the normal staining pattern for claudin-3 and ZO-1, indicating a loss of epithelial integrity, compared with both control and *FZD7*$^{-/-}$/TcdB$_{1–1830}$. Scale bar, 200 μm. Representative images are from one of three independent experiments. **i**, A schematic overview of cellular factors identified in the CRISPR–Cas9 screen. Validated and plausible cellular factors identified in our unbiased genome-wide screens were grouped based on their presence in the same protein complexes and/or signalling pathways. The colour of the gene names reflects the number of unique sgRNAs identified. The arrows link these genes to either confirmed or plausible roles in four major steps of TcdB action: (1) receptor-mediated endocytosis; (2) low pH in the endosomes triggers conformational changes of the TD, which translocates the GTD across endosomal membranes; (3) GTD is later released via auto-proteolysis by the CPD, which is activated by the cytosolic co-factor inositol hexakisphosphate (InsP6); (4) released GTD glucosylates small GTPases such as Rho, Rac, and CDC42.